ISSN 1039-3218

A Transport Model of Port Phillip Bay

S. J. Walker
C. R. Sherwood
C.S.I.R.O. Division of Oceanography
Castray Esplanade, Hobart, Tasmania, Australia

GPO Box 1538, Hobart 7001 Australia

Technical Report No. 39

Port Phillip Bay Environmental Study
CSIRO Environmental Projects Office
Building 9, Forestry Site, Banks Street

Yarralumla, ACT, Australia

PO Box 225, Dickson, ACT 2602 Australia

May 1997

Contents

1 Introduction

This report describes a Transport Model of Port Phillip Bay, and its validation. The model was developed as part of the P8 task in the Port Phillip Bay Environmental Study to simulate the movement of ecologically significant substances (nutrients, pollutants, plankton, fine sediments, ...) around the Bay. It is able to be applied over a wide range of space and time scales, and forms the link between the Hydrodynamic Model (Technical Report 38 - Walker 1997) and the Ecological Model of the Bay (Technical Report 44 - Murray and Parslow 1997). Together, these models form an Integrated Model of the Bay.

The Transport Model simulates the movement of substances (called tracers in this report) around the Bay in accordance with water movements prescribed by the Hydrodynamic Model. The three-dimensional time varying velocity fields resulting from runs of the Hydrodynamic Model are processed to yield time dependent exchanges of water between the cells in the Transport Model. These exchanges represent the effects of both advection and diffusion of material between cells in the water column. The Transport Model implements these exchanges, accounting for the corresponding changes in tracer concentrations. It explicitly simulates physical processes which are not included in the Hydrodynamic Model, such as sources (or sinks) of tracers, sediment transport, exchange of material between the water column and sediments, and mixing within the sediments. Tracer concentrations may also be altered by biological processes in modules which are described in Technical Report 44.

The water column part of the model has been validated (for a conservative dissolved tracer) by simulating salinity in the Bay over the period July 1990 to June 1995. Salinity is not needed by the biological processes in the model, and is included specifically for the purpose of model validation. The sediment part of the model is not well validated, due both to the usual difficulty in obtaining detailed sediment data, and the timing of the physical tasks in the study.

2 Processes

2.1 Introduction

The Transport Model is implemented as a general purpose box model. The region to be modelled is divided horizontally into a number of boxes (polygons), which together exactly cover that region. During the course of the study, a number of model geometries were developed, ranging from a single box covering the whole Bay (the simplest possible model), to a model with 59 boxes covering the Bay. Models with 7, 8 and 59 boxes covering the Bay are shown in Figures 1 to 3.

In each box, the water column is divided into a number of layers. Each layer in a box is called a cell. At the bottom of the water column in each box is a sediment model, which also consists of a number of layers. The Transport Model keeps account of tracer concentrations in each cell of the model, both in the water column and in the sediment. As well, the model includes storage for epibenthic variables at the sediment/water interface, although these variables are only used in the ecological codes. Figure 4 shows the vertical structure of a single box. Note that each box may have different numbers of layers in both the water column and sediments from other boxes. As well, the number of layers in the sediments may vary with time, as sediment is deposited or resuspended.

The set of tracers to be included in the model is determined at run time. In other words, the code (at least, that part of it which implements model input, output, and physical processes) is not written in terms of particular real-world tracers, but processes an arbitrary list of tracers, with behaviour based on a small set of properties defined for each tracer at run time. These include whether a tracer is particulate or dissolved, and if particulate, values such as grain size and grain density. The physical processes which act on the set of tracers included in a given model simulation are described in the following sections.

2.2 Water Column Transport

Movement of water and tracers between cells in the water column of the Transport Model is determined by the velocity field resulting from a run of the Hydrodynamic Model. The primary data used to drive the Transport Model are a specification of all exchanges of water between cells at each time step. These exchanges are calculated from the Hydrodynamic Model results. The Transport Model reads these exchange data at each time step, and implements the exchanges between cells, adjusting tracer concentrations accordingly.

The water column exchanges between Transport Model cells are calculated by tracking very large numbers of particles through the Hydrodynamic Model velocity field (a process which is done while the Hydrodynamic Model is running, as described in Walker (1997)). Particle positions are stored in (very large) output files. For each transport time step, interface software then determines which Transport Model cell each particle starts in, and which cell it ends in. It can then estimate inter-cell exchanges by appropriate book-keeping. These exchange values include the effects of both advection from cell to cell and diffusion between cells. Note that if the time step over which these exchanges are calculated is large, particles may move across several Transport Model cells in a single step, so that non-local transports may occur.

In order to reduce spurious mixing (both vertical and horizontal) in the Transport Model, exchanges are calculated over periods equal or near to a multiple of the dominant tidal frequencies. This minimises oscillatory exchanges between adjacent cells, which would otherwise lead to the model mixing more rapidly, due to the large size of each cell.

The Transport Model extends simulations beyond the extent of the available hydrodynamic data by repeatedly re-using input data in a cyclic fashion. As well, exchange data can be read from a number of input files in a specified sequence, which allows the 'patching' of several shorter hydrodynamic scenarios into a longer set of input data for the Transport Model. At present, exchange data are stored in 6-monthly files, together covering the period July 1990 to June 1995. Long scenarios can be built up from any combination (and repetition) of these files. Fresh-water sources and sinks are automatically combined and repeated in the same manner.

2.3 Horizontal Mixing

There is no explicit horizontal mixing process represented in the Transport Model. In the water column all horizontal mixing is assumed to be included in the exchanges of water from cell to cell which are input from the Hydrodynamic Model results.

In the sediment, it is assumed that there is no direct exchange of tracers between horizontally adjacent cells. This is a good assumption as long as the horizontal extent of each cell is very much larger than the vertical sediment layer spacing, so that horizontal sediment transports happen via vertical exchange with the water column and horizontal movements within the water column. This is true for all envisaged model simulations.

2.4 Vertical Mixing in the Water Column

When the Transport Model is driven using data from the Hydrodynamic Model, vertical mixing is automatically included in the Transport Model by inter-cell exchanges calculated from the Hydrodynamic Model results.

For the purposes of testing the Transport Model and running simple simulations without Hydrodynamic Model input, a constant vertical mixing coefficient, K_z, can be specified for the water column. In this case, the rate of change of concentration C of a tracer with time, due to this process, is given by

$$\frac{\partial C}{\partial t} = K_z \frac{\partial^2 C}{\partial z^2} \tag{1}$$

This equation is cast in centred finite difference form and solved using a weighted average of an implicit scheme and an explicit scheme (usually chosen to be fully implicit).

2.5 Settling

The Transport Model can simulate particulate tracers which have positive or negative settling velocities. Positive values indicate that the tracer is buoyant, and will rise towards the surface layer of the model. Negative values indicate that the tracer will sink towards the bottom of the water column. Any net flux of tracer settling out of the bottom of the water column is usually added to the sediments. This may involve the creation of new sediment layers (discussed in Section 2.6.2). If the properties of a particular tracer are such that it cannot physically enter the sediments (as is the case for some of the organisms included in the ecological module), provision exists in the model for collection in the bottom water column layer, rather than transfer to the sediments.

For a tracer with settling velocity w_s, the rate of change of concentration C due to settling is given by

$$\frac{\partial C}{\partial t} = -\frac{\partial}{\partial z}(w_s C) \tag{2}$$

The settling algorithm integrates fluxes at each layer face using tracer concentrations evaluated over the full distance traversed by a particle in a single time step (in the upwind direction). This correctly handles large settling velocities, or large time steps, where a particle may traverse more than one layer in a single time step. This vertical advection scheme inevitably adds some numerical diffusion, because of the upwind nature of the scheme and the use of a fixed vertical grid with limited resolution. For particular settling velocities (or time step values), where the distance traversed is exactly a multiple of the layer spacing, the scheme is exact.

2.6 Sediment Processes

Amongst the more complex and less well understood processes included in the Transport Model are the resuspension and deposition of sediment. One of the problems in this area is that sediments vary very widely in their physical properties, which means that studies done in one area or on one sediment type are not necessarily relevant to another area or type. There is a wide body of literature available concerning the behaviour of sediments in coastal and estuarine conditions. This report does not attempt to review this area - one starting point for a review of issues related to sediment transport might be Nittrouer and Wright (1994), although that review has its focus on transport across continental shelves, a setting somewhat further offshore than Port Phillip Bay.

The resuspension and deposition model in the Transport Model is largely based on that described in Teisson (1991). However, the physical organisation of the Transport Model sediments is substantially different from the Teisson model. In that model, each layer has a fixed density and residence time, so that the model degenerates to a single layer after a sufficient calm period. This is not acceptable for the Transport Model, which must maintain adequate vertical resolution in the sediments, so that a biogeochemical model (such as that described by Blackburn and Blackburn (1993), for example) can also be implemented as part of the ecological module. The Transport Model thus attempts to maintain fine vertical resolution in the upper sediment layers, deleting or adding layers as sediment is resuspended or deposited. Maximum and minimum desired layer thicknesses can be specified as model parameters.

2.6.1 Sediment Resuspension

Resuspension is the removal of particles from the sea bed by the action of the overlying water. The stress which the water exerts on the sea-bed depends on the nature of the boundary layer at the bottom of the water column. In implementing resuspension, the Transport Model reads spatially varying time series of normalised excess bottom shear stress as input data. These data are calculated using bottom velocity values output by the Hydrodynamic Model, wave data from a wave model, and the wave-current boundary layer model of Madsen (1994). A more complete description of this calculation is found in Section 3.2.

In order to calculate erosion rates, it is necessary to specify properties of the sediment being eroded, and how the rate depends on the applied bed stress. Some authors (for example Lavelle *et al.*, 1984) assume that erosion occurs for all values of applied shear stress, with the rate depending on some power of the stress. Others use a formulation where erosion only occurs when the stress exceeds some critical level, which depends on the properties of the sediment being eroded (Hamblin 1989, Uncles and Stephens 1989, Luettich *et al.*, 1990, Teisson, 1991). The Transport Model calculates the erosion rate E (in ms^{-1}) for the uppermost sediment layer in each box as follows:

$$E = \frac{M}{C}\left(\frac{\tau_{sf} - \tau_c}{\tau_c}\right) \qquad \tau_{sf} > \tau_c \tag{3}$$

Here τ_{sf} is the skin friction component of the bottom shear stress, τ_c is the critical shear stress, C is the mass concentration of sediment ($\mathrm{kg\,m^{-3}}$), and M is an empirically determined erodibility value. Both τ_c and M depend on the properties of the sediment. The quantity in brackets, $\frac{\tau_{sf}-\tau_c}{\tau_c}$, is the normalised excess bottom shear stress, time series of which are read by the model. Because these values are calculated prior to a model run, a side-effect is that the critical shear stress, τ_c, does not vary with time in the model, but is specified (in a spatially varying way) when calculating excess bottom shear stress values (Section 3.2). Values are typically of the order of $0.1\mathrm{Nm}^{-2}$.

Determination of the value of M is not an easy task. Teisson (1991) uses a formulation where the erodibility depends on the concentration as follows:

$$M = 0.55\left(\frac{C}{1000}\right)^3 \quad \mathrm{kg\,m^{-2}s^{-1}} \tag{4}$$

A short review of literature values of M is given in Uncles and Stephens (1989). Their model uses a value of about $3 \times 10^{-5}\mathrm{kg\,m^{-2}s^{-1}}$, but they note that other authors use values ranging from 1.7×10^{-5}kg m^{-2}s^{-1} to 3×10^{-3}kg m^{-2}s^{-1}. For $C = 200$kg m^{-3}, (4) gives a value of 4.4×10^{-3}kg m^{-2}s^{-1}. Uncles and Stephens note that muds with high M values tend also to have high τ_c values. Delo (1988) (cited in Uncles and Stephens (1989)) suggests that M should be related to τ_c as follows:

$$M = 0.002\tau_c \quad \mathrm{kg\,m^{-2}s^{-1}} \tag{5}$$

All of the above values refer to fine sediments (muds) from various estuaries around the world. In the absence (at present) of suitable observations from Port Phillip Bay, the Transport Model uses (5) to calculate M. The values for M (and τ_c above) thus do not properly take into account the mixed nature of the bed, or changes in bed composition over time.

2.6.2 Sediment Deposition

When sinking particles reach the bottom of the water column, they may be deposited on the sediment surface. The way in which deposition proceeds depends heavily on the nature of the particles involved. Flocculation leads to larger aggregate particles which may fall faster. As concentrations near the bed become large, the upward expulsion of entrained water may slow the settling process (hindered settling). These effects can be represented to some extent by making the fall velocity depend on concentration (Uncles and Stephens 1989, Teisson 1991). At present, for simplicity, processes such as flocculation and hindered settling are not represented in the Transport Model. As well, during deposition, it is assumed that each particulate tracer behaves in a manner which does not depend on other tracers which may be present. This may not be a particularly good assumption when mixtures of sediment types with very different properties are present.

As well as settling velocity, each particulate tracer in the Transport Model has a specified particle size, grain density, and initial deposit density. When particulate tracers are to be deposited, the thickness of the new deposit is calculated using by summing the deposit thickness for each individual tracer, calculated using the initial deposit density specified for that tracer. An amount of pore water will become trapped in the new deposit as it forms. This water is assumed to come from the lowest water column layer. The amount of water trapped will depend on the porosity of the new deposit, which can be calculated from the initial deposit density and the tracer grain density.

As sediment deposits, the uppermost sediment layer increases in thickness until it reaches a specified limit. Beyond that, a new surface sediment layer is created. This process can continue until some maximum number of layers is reached. Then the model will coalesce deep sediment layers to allow the creation of new surface layers. This is done to preserve depth resolution near the surface, at the expense of resolution deeper in the sediment.

The process of compaction of sediments following deposition is not currently represented in the Transport Model.

2.7 Vertical Sediment Exchanges

Vertical mixing and transport of tracers in the sediment layers of the Transport Model is performed by a number of processes, of both physical and biological origin. Each process included in the model is described in detail in separate sections below.

The rates at which biological mixing processes occur at a point in the sediments is assumed to be dependent on the density of animals (number per square meter) and the depth within the sediments to which these animals are active. These quantities are represented by two model variables - the depth-integrated density of animals, and a representative sediment mixing depth. Each of these variables may vary in time and space, and are available to be modified by the biological module if required. This is probably a more sophisticated representation than is warranted by available data, and in fact no simulations have yet been performed where these values have been altered over time. These values are thus currently fixed for each run, and hence take on the role of model parameters.

Each biological mixing process is described by a single parameter, which is the process rate per animal per square meter at the sediment surface. The depth dependence of the mixing process rates is described by a single simple functional form. Thus, the depth dependence of a process in a box with A animals per square meter is given by

$$R(z) \propto AKf(z,\sigma) \tag{6}$$

where $R(z)$ is the process rate at depth z below the sediment surface, K is the total process rate per animal per square meter at the sediment surface and σ is the mixing depth in that box. The Transport Model can implement constant, linear, parabolic and half-Gaussian forms for $f(z,\sigma)$.

2.7.1 Bioirrigation

Bioirrigation is the movement of water within the sediments and exchange with the overlying water column due to biological activity. Because different species have quite different behaviour, it may be necessary to implement a range of processes which move water in different ways. Three processes have been included in the Transport Model. They are diffusion, exchange and injection. Diffusion mixes pore water between adjacent layers within the sediments. Exchange moves water between the overlying water column and each sediment layer directly. Injection 'pumps' overlying water into each layer, with a compensating upward flow of pore water (in order to conserve volume). A schematic for each process is shown in Figure 5.

2.7.1.1 Diffusion

Diffusion of pore water induced by bioirrigation is represented in a similar way to vertical mixing in the water column. For a tracer with concentration C, we have

$$\frac{\partial C}{\partial t} = \frac{\partial}{\partial z}(K_z \frac{\partial C}{\partial z}) \tag{7}$$

where

$$K_z(z) = AKf(z,\sigma) \tag{8}$$

as outlined above.

This formulation assumes that the sediment porosity is constant with depth, possibly a somewhat unrealistic assumption.

2.7.1.2 Exchange

This process represents direct exchange between the bottom water column layer and the pore water in each of the underlying sediment layers. For a tracer with concentration C_w in the bottom water column layer, and C_i in the i'th sediment layer pore water, we have

$$\frac{\partial C_w}{\partial t} = \frac{1}{V_w}\sum_{i=i_{top}}^{N} R_i(C_i - C_w) \quad (9)$$

$$\frac{\partial C_i}{\partial t} = -\frac{R_i}{p_i V_i}(C_i - C_w) \quad (10)$$

where V_w is the volume of the bottom water column layer, N is the number of sediment layers, i_{top} is the index of the uppermost sediment layer, V_i is the volume of the i'th sediment layer, p_i is the porosity of the i'th sediment layer, and R_i is the exchange rate between the bottom water column layer and the i'th sediment layer, given by

$$R_i = \frac{AKf(z(i),\sigma)}{\int_{-\infty}^{0} f(z,\sigma)dz} \quad (11)$$

as discussed above. Note that i increases with depth in the sediment. This leads to a system of differential equations which theoretically can be solved simultaneously. However, for simplicity, and to minimise computational cost, we assume that the bottom water column layer exchanges with each of the sediment layers in turn, rather than with all layers simultaneously. This is a good approximation as long as the water column layer has a much larger volume than the pore water in any of the sediment layers, and as long as exchange rates are small. The solution for each exchange can then be expressed analytically, as follows:

$$C_w(t+\Delta t) = (C_w(t) - C_e)e^{-k\Delta t} + C_e \quad (12)$$

$$C_i(t+\Delta t) = C_i(t) - \frac{V_w}{p_i V_i}\left(C_w(t+\Delta t) - C_w(t)\right) \quad (13)$$

where $C_e = (V_w C_w(t) + p_i V_i C_i(t))/(V_w + p_i V_i)$ and $k = R_i(\frac{1}{V_w} + \frac{1}{p_i V_i})$. These solutions are applied sequentially, starting with the uppermost sediment layer and progressing downwards. C_w is updated after each layer.

2.7.1.3 Injection

This process injects water from the bottom water column layer into each of the sediment layers. The pore volume in each sediment layer does not change, so that after mixing within the layer is calculated, excess water percolates into the layer/s above. Eventually, a volume of water equal to the total volume injected percolates out of the sediment surface back into the bottom water column layer. With variables as defined above, we can express the tracer concentration in the i'th sediment layer at the end of a time step as follows:

$$C_i(t + \Delta t) = C_i(t) + \frac{1}{p_i V_i} \left(C_w R_i \Delta t + C_{i+1}(t + \Delta t) \sum_{k=i+1}^{N} R_k \Delta t \right) \quad (14)$$

As implied in the formulation, this calculation starts at $i = N$, and proceeds sequentially upwards through the sediment layers. At the sediment surface, we have

$$C_w(t + \Delta t) = C_w(t) + \frac{I}{V_w} \left(C_{i_{top}} - C_w(t) \right) \quad (15)$$

where I is the total volume of water injected into the sediments in a time step ($I = \Delta t \sum R_i$).

2.7.2 Bioturbation

Bioturbation is the movement of particulates within the sediments due to biological activity. Again, because different species have quite different behaviour, it may be necessary to implement a range of processes which move particulates in different ways. Three processes have been considered for included in the Transport Model. They are diffusion, exchange and expulsion. Diffusion mixes particles between adjacent layers within the sediments. Exchange moves particulates between the sediment surface and deeper layers. Expulsion removes particles from each sediment layer and deposits them on the sediment surface. These processes, unlike bioirrigation, may alter the volume of a particular layer. A schematic for each process is shown in Figure 6.

At present, none of these processes have been implemented in the Transport Model.

2.8 Atmosphere-Water Exchange

The Transport Model includes a process which simulates the exchange of gases between the atmosphere and the surface layer of the water column. It is assumed that a gas is freely available in the atmosphere as an 'infinite' source (in other words, the atmospheric concentration is constant over time, so that the process would eventually lead to saturation in the water column in the absence of any other processes). The surface flux F is given by

$$F = -\frac{K}{dz}(G - S) \tag{16}$$

where K is the diffusion coefficient (molecular diffusion), G is the gas concentration in the surface water layer, S is the saturation concentration, and dz is a small stagnant layer thickness. In general, K and S vary with temperature, and dz varies with wind speed and surface conditions (presence of slicks etc). However, at present, these values are held constant in the Transport Model.

The rate of change of gas concentration in the surface layer is given by

$$\frac{\partial G}{\partial t} = -\frac{K}{Ddz}(G - S) \tag{17}$$

where D is the thickness of the surface layer. This equation implies that G exponentially approaches S (it is equivalent to a decay equation in $(G - S)$, assuming that S remains constant over a time step). The model calculates G at each time step analytically:

$$G(t + dt) = (G(t) - S)\exp(-\frac{Kdt}{Ddz}) + S \tag{18}$$

At present, the only gas included in the model is Oxygen, with the following constant exchange parameters:

$$K = 2 \times 10^{-9}\ \mathrm{m^2 s^{-1}} \tag{19}$$

$$S = 8000\,\mathrm{mg\,m^{-3}} \tag{20}$$
$$dz = 2 \times 10^{-5}\ \mathrm{m} \tag{21}$$

2.9 Decay

To allow the simulation of radioactive tracers (or other tracers with some first-order loss), the Transport Model incorporates a decay process. According to this process, a tracer which has a non-zero decay constant k, will have its concentration C reduced at a rate given by

$$\frac{\partial C}{\partial t} = -kC \tag{22}$$

This can be solved analytically, so that the concentration after a time step of Δt seconds is given by

$$C(t + \Delta t) = C(t)e^{-k\Delta t} \tag{23}$$

3 Inputs

3.1 Transport

The primary Transport Model input consists of inter-cell exchanges of water, calculated by particle tracking within Hydrodynamic Model runs. There is a potentially serious problem concerning the amount of exchange data to be transferred. For example, a model implementation with 100 boxes covering the Bay and 10 layers in the water column has 1000 cells, which means that there are theoretically of the order of 10^6 inter-cell exchange values for each time step. This problem rapidly worsens as the model size grows, since the number of values potentially scales as the square of the number of cells. The problem is largely caused by the ability of the model to use large time steps, leading to non-local transports. It is addressed by assuming that the actual number of destination cells for water from a given cell is relatively small for any one time step. Exchanges of water out of each cell are ranked in magnitude, and only the most significant are transferred, up to some maximum number of values. This maximum number can be chosen to minimise errors, or minimise data size. For most reasonable simulations, it has been found that the maximum number chosen is sufficient to represent all non-zero exchanges from each cell, so that no errors occur.

A mechanism is provided to allow the model to avoid some boxes when performing calculations, so that concentrations in those boxes do not change their properties over time (or else only change in some explicitly specified way). These boxes are known as 'boundary' boxes. In the Port Phillip Bay model, Bass Strait is represented by a single boundary box. Exchange between the Bay and Bass Strait is thus automatically included in the exchange inputs to the model, as the particle tracking calculations in the Hydrodynamic Model include this area.

3.2 Bottom Stress

A time series of daily- and spatial-mean excess bottom shear stress was calculated for the 59-box model geometry for the period 1 July 1991 to 31 June 1995, inclusive. Excess bottom shear stress, S, is given by $S = \frac{\tau_{sf} - \tau_c}{\tau_c}$, where τ_{sf} is the skin-friction component of total bottom shear stress (the other component is form drag caused by bedforms or biogenic bottom-roughness features), and τ_c is the critical shear stress for erosion. The τ_{sf} used in sediment transport calculations is the spatial/temporal maximum over wave periods and local topography. The calculations used time series of hourly bottom current velocity (produced as output from the bottom cells of the Hydrodynamic Model), hourly wind velocities used to force the Hydrodynamic Model, water depths from the Hydrodynamic Model, and bottom sediment characteristics (as interpreted over Transport Model boxes) from PPBES Task P7 data (Greilach *et al.*, 1996) and Beasley (1966). A two-hourly time series of τ_{sf} was computed on the 1000m

Hydrodynamic Model grid, from which the daily and box-mean values of S were computed. Calculations leading to estimates of τ_{sf} are described below.

Wind fetches to each Hydrodynamic Model gridpoint were calculated for 16 wind directions. For any direction, the fetch was taken as the distance to the first (closest) upwind intersection with the coastline. Fetches in each of the 16 tabulated directions were weighted averages of 35 calculations about a 45-degree arc centred on that direction. Weighting was proportional to $\cos^2(|a - da|)$, where a is the principal direction, and da is the deviation, ranging up to ± 22.5 deg.

There is no rigorous justification for the fetch weighting scheme. The *Shore Protection Manual* (CERC, 1984) states that the effective fetch calculations previously used in narrow lakes (which involve cosine weighting over a +-90 degree arc) should not be used with the revised wave-growth curves because the directional distribution of wave energy at the spectral peak frequency is very narrow, closer to $\cos^{10}()$. This, however ignores spreading caused by shoaling, refraction, and diffraction that occurs in shallow areas like Port Phillip Bay. The present, admittedly heuristic, scheme produces fetchs that look reasonable, smooth out the windward shoreline, and allow some wave energy to propagate up to about 22.5 deg around corners. Restriction to a narrow angular range about the principal axis ensures that fetches are not greatly biased by the averaging technique.

At each two-hourly time interval, and at each Hydrodynamic Model grid point, wind speed and direction were obtained from the Hydrodynamic Model forcing data (described in Walker 1997). Fetch was then determined from the calculated values described above using linear interpolation in direction. Depth limited, fetch limited, fully developed (time unlimited) significant wave heights H_s and dominant (modal) periods T_m were then calculated for local water depth according to Eqns. 3-39 and 3-40 in *The Shore Protection Manual.* Near-bottom wave-orbital velocities were calculated for monochromatic waves using linear wave theory (Komar, 1976, for example). Wave direction was assumed to be the same as the wind direction. As as example of the above calculations, Figures 7 to 10 show fetch, wave height, wave period and bottom orbital velocities calculated during strong south westerly winds (about 17 m/s from 230°) at 1600 on 19 September 1994, at a time when the SEDCAM instrument was located near Red Bluff in the north east of the Bay.

Bottom shear stresses were calculated from the near-bottom wave-orbital velocities and Hydrodynamic Model bottom currents according to the wave-current bottom-boundary layer model of Madsen (1994). Movable bed roughness for the calculations depended on flow conditions and local sediment characteristics, which were assigned according to task P7 data in each of the 59 Transport Model boxes. The stress calculations required a roughness parameter, k_b, which was set equal to $z_{o_{out}}/30$, where $z_{o_{out}}$ is outer bed roughness length used to represent ripples or biogenic roughness elements. Because $z_{o_{out}}$ depends on bottom stress, and stress is quite sensitive to bottom roughness, the stress/bottom roughness calculations were iterative. When flow conditions were below the threshold of motion, bed roughness elements everywhere were arbitrarily assigned characteristic height $n = 0.5$cm and length $l = 20$cm, and $z_{o_{out}} = n^2/l$ or 0.0125cm (Grant and Madsen 1982, Wiberg and Harris, 1994).

Inner roughness was set at $z_{o_{in}} = D_{50}/30$ or 0.005cm, whichever was greater, where D_{50} is the median grain size in centimetres. When the critical shear stress for erosion was exceeded, bed roughness depended on grain size and transport stage. Where local sediments had median grain size coarser than 3 phi (0.0125cm) and silt+clay content less than 10%, equilibrium ripple dimensions were calculated (Wiberg and Harris, 1994) and $z_{o_{out}} = n^2/l$. Where sediments were very fine sand (finer than 3 phi) or silt+clay content exceeded 10%, a biogenic roughness formulation recommended by Wiberg (pers. comm., 1994) was used. This formulation assumed that the maximum roughness of $z_{o_{out}}$, caused by biogenic mounds, pits, tracks, and trails, occurred at low flow, and decreased as these features were smoothed away with increasing transport stage. The formulation for steepness of biogenic roughness elements is:

$$\frac{n}{l} = \exp(-1.67 \log(t_*) - 4.11) \qquad (24)$$

where

$$t_* = \frac{\rho u_*^2}{((\rho_s - \rho) g D_{50})} \tag{25}$$

is the non-dimensional Shields parameter, $u_* = \sqrt{\tau_{sf}/\rho}$ is the friction velocity, ρ is the water density, ρ_s is sediment density, g is the gravitational acceleration, and D_{50} is the median grain size. The biogenic roughness calculation presupposes a wavelength l (which equals 20 cm here) for bottom features and calculates n from the steepness n/l, with the additional constraint that n/l be less than some maximum value (0.5/20 here) under low-flow conditions. Bottom roughness is then calculated as $z_{o_{out}} = n^2/l$.

When roughness elements were present, a form-drag correction was made according to Smith and McLean (1977) to separate the skin-friction component of bottom stress, τ_{sf}. Bedform drag coefficient for these corrections was assumed to be 0.5. Inner bed roughness $z_{o_{in}}$ was assumed to be the greater of the Nikuradse roughness, the sediment-transport roughness (Wiberg and Rubin, 1989), or 0.005cm. When ripples or biogenic roughness features were flattened during upper plane-bed transport conditions, the inner no form-drag correction was needed, and $z_{o_{out}} = z_{o_{in}} = z_{o_{ST}}$, the sediment-transport roughness. Finally, the maximum value of skin friction τ_{sfmax}, which occurs at the crest of the roughness elements and where most material is suspended, was computed (Wiberg *et al.*, 1994).

In practice, the downward adjustment from τ_b to τ_{sf} to account for form drag is a factor of about 0.6, and is almost entirely offset by the upward adjustments to τ_{sfmax}. However, the calculations remain very sensitive to bed roughness. The values chosen here are reasonable guesses based on experience elsewhere (e.g., Wiberg *et al.*, 1994; Sherwood, 1995).

All wave, orbital velocity and shear stress calculations described above assumed that the system had reached a steady state with respect to the forcing being applied. To complete the calculation of excess shear stress, estimates of critical shear stresses τ_c were required. These were calculated for representative sediment types in each of the 59 model boxes using the non-dimensional Shields curve (White 1970, Smith 1977) for non-cohesive sediments using the median grain diameter and assuming a density equal to that of quartz. Representative sediment types in each box were inferred from P7 data. Where several samples were available in a single box, a representative sample was chosen by considering sample depth and box-mean depth, and the distribution of available samples. When no samples were available in a model box, values from an actual sample obtained elsewhere were assigned, guided by Beasley's (1966) sediment-type maps. A minimum critical shear stress of 0.09 N/m2 was assigned to the finest sediments, based on the assumption that cohesion would affect erodibility of these muds. However, the estimates of critical shear stress are probably low where microphytobenthos, bacteria, sub-areal exposure, compaction, or high clay content act to increase cohesion.

The calculation of excess shear stress does not include sediment induced stratification, which may alter the stress felt by the bed and hence alter erosion rates (see, for example, Glenn and Grant, 1987, Sheng and Villaret, 1989, McLean 1992).

3.3 Sources and Sinks

These data describe the fluxes of tracers which occur between the model and the external environment. There are two classes for these data, one for data associated with a particular location (for example rivers, drains, pipes, open boundaries) and one for data covering the entire area of the model (for example rain, aerosols etc). These data are time dependent within each run. For simplicity, it is assumed that there are no sources or sinks directly to or from the sediment layers of the model. As a result, new particulate matter only reaches the sediment by sinking, after having been added to (or created in) the water column.

As far as the physics of the model are concerned, the only significant sources are those for fresh water, salt and possibly heat. These are described below. Sources and sinks of ecologically significant tracers (nutrients, for example) are described in Technical Report 44 (Murray and Parslow 1997).

3.3.1 Fresh Water

In order to maintain consistency between the Hydrodynamic Model and the Transport Model, it is necessary to use identical fresh-water inputs in both models. Freshwater forcing for both models consisted of data describing rainfall, evaporation, and flow data for the major rivers, creeks and drains. These data were obtained primarily from the Bureau of Meteorology, the Victorian EPA and Melbourne Water. In both models, all freshwater inputs (rain and flows from rivers, creeks and drains) were assumed to have zero salinity. The inputs from rivers, creeks and drains were located in the model grid at the box nearest their actual locations around the Bay. Rainfall and evaporation were applied over the surface of the Bay according to their observed distributions.

A detailed description of all fresh water model inputs can be found in Technical Report 38 (Walker 1997).

3.3.2 Salt

Salinity is not an important variable in the Transport Model. Its effects on water density and hence dynamics are represented in the Hydrodynamic Model results. It is not used by the ecological processes represented in the model. Nevertheless, it was included as a model variable, as it is dissolved and conservative, and hence a good tracer with which to validate the water column part of the model. Salinity varies over both space and time in the Bay, and was extensively measured during the study.

The only source of salt considered in the model is sea water. Thus, it was necessary to specify the salinity of the Bass Strait boundary box in the model. As for the Hydrodynamic Model, a constant value of 35.4 was chosen for all simulations.

3.3.3 Heat

Like salinity, temperature is not an important variable in the Transport Model. Again, its dynamical effects are represented by virtue of their inclusion in the Hydrodynamic Model results. It does play an important part in the ecological modules, however, controlling processes such as plankton growth. For simplicity, the ecological modules assume a simple seasonal variation of water temperature in the Bay, which is adequate for their purposes (Technical Report 44 - Murray and Parslow 1997). This avoids having to reproduce a complex surface heat flux module in the Transport Model. Such a module is included in the Hydrodynamic Model (see Technical Report 38 - Walker (1997) for details), so that events such as thermal stratification on the Bay are properly represented by the alterations they cause to vertical exchanges passed from the Hydrodynamic Model to the Transport Model. As a result of these considerations, temperature is not included as a tracer in the Transport Model.

3.3.4 Sediments

Although the Transport Model contains some quite detailed processes relevant to sediment transport, a limiting factor in the development of the sediment part of the model has been a lack of forcing, initialisation and validation data related to sediments. As a result, this part of the model is significantly less well tested and developed, compared to the water column part. Issues related to these difficulties are discussed below.

As stated in the PPBES final report (Harris *et al.*, 1996), inputs of particulates enter the Bay from a number of sources. No data is available for inputs from coastal erosion, or from Bass Strait. Other inputs are dominated by the Yarra river. Estimates undertaken as part of the study show a total non-filterable residue (NFR) input of about 145000 tonnes over the period January 1993 to October 1995 (inclusive), which corresponds to an annual average of about 51000 tonnes. Average figures do not give a good idea of the variations in input, however, and closer examination of the data shows that most input occurs in just a few short events.

Particulate inputs from rivers, creeks and drains (excluding the Yarra and WTC) are described in Technical Report 12 - NSR Pty Ltd (1993). These data show a total annual input of about 14000 tonnes NFR from these sources, based mainly on an analysis of historical data collected from 1979 to 1981. Atmospheric inputs of particulates are roughly estimated by Hunter (1992) (Technical Report 9) to be about 13000 tonnes per year, based on atmospheric concentrations of particulates given in Beer *et al.*, (1992). Total suspended solids data obtained from the Werribee Treatment Complex show an annual input of about 6000 tonnes.

The total of all the above inputs comes to about 85000 tonnes per year. However, if spread evenly over the Bay, these known inputs account for perhaps as little as one tenth of the (long-term) sedimentation rate (estimated as about 0.3 mm/year in Harris *et al.*, 1996). In other words, there is insufficient data to allow particulate inputs into the Transport Model to be specified with any degree of confidence. In the light of this, the approach taken to date has been to ignore such inputs, on the basis that Transport Model simulations have so far been carried out for periods of up to 10 years or so. Over periods of this order, it has been assumed that sediment movements in the Bay are dominated by transports of existing sediments rather than the addition of new sediments. As well, dredging and other engineering works are not represented in the model.

Physical measurements of sediments undertaken during the study included the collection and analysis of cores from 80 sites in the Bay. The cores were analysed for grain size, density, porosity, viscosity, permeability and consolidation characteristics. These data are presented in Greilach *et al.*, (1996), and form the basis for initialising the sediment properties of the Transport Model. Unfortunately, these data do not include detailed information on sediment properties as a function of depth, so that the way in which sediments are initialised in the Transport Model does not include any depth variation. Only limited work has been done on the most effective way to initialise the model with these data. Significant issues here, on which further work is required, include extrapolation from each core site to the box structure of the model, and the most appropriate choice of size classes to be represented in the model.

As presently configured, the Transport Model uses seven size classes for inorganic particulate tracers. These range in 1 phi steps from 1 phi (coarse sands) to 7 phi (fine silts), with settling velocities ranging from about 0.06m/s to about 0.00004 m/s (Table 1).

Size class (phi)	Grain size (mm)	Settling velocity (m/s)
1	0.5	0.065
2	0.25	0.027
3	0.125	0.0096
4	0.0625	0.0030
5	0.031	0.00079
6	0.016	0.00019
7	0.0078	0.000042

Table 1: Inorganic particle grain sizes and settling velocities.

In each model box, an initial sediment deposit is created, usually consisting of a number of layers, which has a mixture of these classes, according to data from nearby core sample sites.

3.3.5 Other Tracers

The details of inputs for most other model variables can be found in Technical Report 44 - Murray and Parslow 1997. All model variables are allowed to have both point and diffuse sources located in the Bay. However, the physical side of the Transport Model is largely oblivious to the specific set of tracers being modelled. One special case worth mentioning here is Oxygen, which exchanges with the atmosphere at the water surface. The exchange process is described in Section 2.8.

4 Model Validation

During the course of the study and the development of the Integrated Ecological Model, the Transport Model was implemented for Port Phillip Bay with a number of geometries. In terms of horizontal resolution, these ranged from a single box covering the entire Bay, up to a model with 59 boxes in the Bay (Figures 1 to 3). In terms of vertical resolution, the models ranged from having 1 layer in each of the water column and sediments, through to having 5 water column layers and several (time varying) sediment layers. This section describes the performance of the physical (non-biological) part of these models, assessed against available observational data.

4.1 Mass Conservation

The Hydrodynamic Model includes a continuity equation which enforces incompressibility - that is, cells in the Hydrodynamic Model do not change their volume (except possibly the surface cells, where the surface elevation may change over time, due to tidal or other effects). If the Transport Model and Hydrodynamic Model had identical cell structure, then the exchange transferred by the interface software should ensure continuity in the Transport Model. In general, however, the Transport Model has different cell structure to the Hydrodynamic Model. As well, exchanges are calculated in a Lagrangian manner (using particle tracking), rather than the Eulerian scheme used to preserve continuity in the Hydrodynamic Model, and these schemes do not in general produce exactly the same results. Both these factors mean that the fluxes transferred to the Transport Model can cause cells within the water column to change their volume in ways which do not entirely correspond with Hydrodynamic Model changes.

In the Transport Model, cell volumes change over time in response to any net exchanges of water from cell to cell, and any sources or sinks of fresh water (such as rainfall, evaporation, rivers etc). For consistency, it is necessary that the Transport Model use the same fresh water source and sink data as were specified in the Hydrodynamic Model simulations. Even when this is done, it has been found that volumetric errors sometimes occur in the Transport Model due to unavoidable errors in the exchange data. These have been observed primarily in cells in the Sands region, where flow velocities are high, bathymetry is complex, and the Eulerian and Lagrangian schemes differ most. They are controlled by arbitrarily re-setting cell volumes to a default value if they exceed specified bounds. This adjustment procedure is designed to conserve concentration, and hence does not conserve mass. Over the main body of the Bay, this procedure occurs infrequently. As well, the errors appear to be fairly randomly distributed in space, so that volume corrections in one box often tend to be cancelled by opposite corrections of similar magnitude in nearby boxes. In any case, this correction procedure does not appear to unduly affect model results, as demonstrated by the salinity results described in following sections. Nevertheless, the use of particle tracking to couple the Hydrodynamic Model to the Transport Model, while allowing a great deal of flexibility, needs further development work to minimise or eliminate the need for cell volume adjustments.

4.2 Exchange with Bass Strait

The 'flushing time' of the Bay is of interest because it is one of the factors which determine concentrations of substances in the Bay. However, the flushing time (with respect to Bass Strait) varies from place to place in the Bay. For example, a water parcel originating in the south of the Bay near the Rip will exchange with Bass Strait quite quickly (leading to the high exchange ratios found by the Phase 1 drogue study (MMBW/FWD 1973)). A water parcel located in the centre of the Bay will exchange with Bass Strait much more slowly, and one in Corio Bay more slowly still. A number of estimates of flushing time for the Bay as a whole are quoted by Hunter (1992), ranging from about 300 to 480 days.

CTD surveys in the Sands area were conducted during the period 7 - 11 May 1994, in conjunction with HF-Radar (Prytz and Heron 1995 -

Technical Report 19) and ADCP measurements. Transects were located at the northern and southern edges of the Sands and along the West, Symonds and South Channels through the Sands. The flushing time of the Bay was estimated from CTD and ADCP data by calculating salt and water fluxes at the southern end of the channels through the Sands (Pattiaratchi *et al.*, 1996 - Technical Report 34). This calculation was done for two periods, each covering a single tidal cycle, on the 7th and 10 May. For the 7th May, the tidal range in the Bay was 0.28m and the calculated flushing time was about 380 days (this is the value quoted in Harris *et al.*, 1996). For the 10th May, the tidal range in the Bay was 0.45m, and the calculated flushing time was about 340 days. The mean tidal range in the Bay is about 0.45m (calculated from Hovell Pile data during 1994), so that the estimate for the 10th May is likely to be better than that for the 7th May. Errors in the ADCP flow data appear to be about 10% (based on comparisons of time integrated flow values and sea-level changes inside the Bay), which yields an uncertainty in these flushing time estimates of about 40 days. Sea level also varies as a result of lower frequency effects, which may further add to exchange with Bass Strait. Other processes (rainfall, evaporation, runoff) may also make a small contribution to flushing. The flushing times above are thus probably somewhat of an overestimate, with an uncertainty of somewhat more than 40 days.

For flushing tests of the Transport Model, the 7-box, 8-box and 59-box models were initialised with a conservative tracer with a concentration of 1 everywhere inside the Bay, and 0 in Bass Strait (in arbitrary units). The models all represented the water column as a single layer in the vertical. The models were run using inter-cell exchanges calculated from the Hydrodynamic Model for calendar 1994, as well as fresh-water inputs for that year, as described above. During the simulations, tracer concentrations decreased in each cell in the Bay, due to exchange between the southern portion of the Bay and Bass Strait, and transport within the Bay. For each cell in the Bay, a 'flushing time constant' was calculated by fitting an exponential decay curve to the tracer concentration C as follows:

$$C = C_0 \mathrm{e}^{-kt} \qquad (26)$$

where here $C_0 = 1$, and the flushing time is given by $\frac{1}{k}$. Note that this is a slightly different analysis to that used in Harris *et al.*, 1996, which is why the flushing times there differ slightly from those given here. The flushing times also depend to some extent on the period modelled, due to differences in exchange and forcing data.

The flushing behaviour of the 7-box model is shown in Figure 11. For this model, all boxes have a flushing time close to 93 days, except for box 1. In box 1, the tracer concentration shows more complex behaviour, due to the fact that it has strong tidal exchange with Bass Strait, and the 24 hour model timestep (and Hydrodynamic Model exchange calculations) alias the tidal signal. The aliased signal appears as an oscillation in concentration values with a period of about 15 days. The short flushing time of this model compared to observed values is due to the coarse resolution of the model.

The flushing behaviour of the 8-box model is shown in Figure 12. For this model, all boxes have a flushing time close to 172 days, except for boxes 1 and 2, which again show a strong tidally aliased signal. A significant result here is that the addition of another box in the Sands region almost doubles the flushing time of the model. This is because the area to the south of the Sands does exchange rapidly with Bass Strait, but the main body of the Bay does not. If a model is to represent this gradient in exchange, then it needs adequate resolution in the Great Sands area.

The 59-box model shows a wider range of flushing times, from near zero at the Rip, to about 315 days in Corio Bay. The bulk of the boxes in the main body of the Bay show flushing times of between 260 to 280 days. Figure 13 shows a spatial plot of flushing times in the 59-box model. Again, boxes near the entrance to the Bay show oscillations in concentration due to aliasing of the tidal signal. Flushing times shown in these boxes are small, but inaccurate (the high levels of noise affects the exponential fitting process).

It is obvious from the above results that the flushing time of the Transport Model depends strongly on the horizontal resolution of the model, particularly in the area including the Rip and Great Sands. For most ecological simulations, the 59 box model of the Bay was used, which means that these simulations incorporate a flushing time for the main body of the

Bay of about 270 days. This is about 80% of that observed (assuming an observed value of 340 days - the result from the 10th May estimate described above). Further refinement of the model geometry in the Sands region might increase this value, at the expense of some added computational effort and exchange file size.

The impact of this reduced model flushing time on ecological simulations of the Bay is not expected to be large. In both the model and reality, the flushing time of the Bay is much longer than the time scales of ecologically significant phenomena like input events and blooms, but is similar to seasonal and annual time-scales. Consider the case of a 'conservative', dissolved tracer (in the ecological context, phosphorus is a reasonable example in Port Phillip Bay). At steady state, the input rate to the Bay must equal the rate of loss of material by exchange with Bass Strait. It is easy to show that, at steady state, the 59 box model will (assuming a uniform Bay) predict a concentration which is about 80% of that which should be observed. This concentration represents a total dissolved mass equivalent to the input summed over a period equal to the flushing time. However, for ecologically significant tracers (nitrogen, for example), there are many other processes affecting water column concentration. The total dissolved mass is often very much less than the input summed over the flushing time, so that loss due to flushing is a small term in the overall behaviour of the tracer (and the model induces a roughly 20% error in that term). Flushing again becomes significant when concentrations become large, so that simulations which show the Bay becoming eutrophic may lose somewhat more material to flushing than they should.

4.3 Salinity

Salinity in the Bay is modified by three competing effects. The first is freshwater input from rain, rivers, creeks and drains. This always tends to reduce salinity in the Bay. The second effect is evaporation, which always tends to increase salinity in the Bay. The third effect is exchange with Bass Strait, which increases salinity in the Bay when the Bay salinity is lower than that in Bass Strait, and decreases salinity in the Bay when the Bay salinity is higher than that in Bass Strait.

Model performance tests for the water column consisted of simulations of salinity over the 5-year period July 1990 to June 1995. For these simulations, the 59-box model geometry was used. Exchange and freshwater inputs were as described above, except for experiments with rainfall and evaporation rates described below. Field measurements were available from 6 sites (designated 1, 4, 6, 9, 11 and 13) around the edge of the Bay, occupied at roughly fortnightly intervals by VFRI since March 1990. As well, field data from 2 sites (MW1 and MW2) closer to the Bay centre were available for the period January 1993 to mid 1995, and 3 further sites (N1 to N3) for shorter periods during the study. The locations of these sites are shown in Figure 14.

Initially, simulations were carried out using freshwater input data as obtained by the study (and described above). The resulting modelled salinities are compared with measurements in Figure 15. It is obvious that the model does not reproduce realistic salinity values with this input data. The modelled values are too high at all times and at all sites. As a result, a number of further simulations were performed, varying either evaporation or rainfall rates, in an attempt to achieve improved salinity values. River flow rates were not altered, as they are considered the most reliable of the fresh-water data. As well, altering them changes the dynamics of the system, requiring recalculation of exchanges with the Hydrodynamic Model. However, moderate changes in rain or evaporation are expected to have small dynamic effect within the Bay, so that the Hydrodynamic Model exchange inputs were not modified for the simulations discussed below. Model flushing time is also an issue for salinity, but cannot be altered without altering model geometry. Flushing effects are discussed further below.

Figure 16 shows results for a simulation where evaporation rates have been uniformly scaled by a factor of 0.7. The modelled salinities here are much closer to those measured. This is also true in a simulation where rain is uniformly scaled by a factor of 1.6, shown in Figure 17. Note that the long term rain rate (about 650mm/year) is about half the evaporation rate (about 1400mm/year) in Port Phillip Bay, so that the gross similarity of these two simulations is not surprising (a 30% reduction in evaporation being roughly equivalent in the Bay to a 60% increase in rainfall, disregarding spatial distribution effects). The fact that decreasing evaporation or increasing rainfall results in much improved model salinities points to possible problems with either the freshwater input data, or model flushing.

Firstly, consider flushing in the model. It has already been established that this 59-box model has a flushing time for the main bulk of the Bay of about 270 days, about 20% less than observed estimates (which we will take to be 340 days here). Consider a situation where the bulk of the Bay has a salinity about 1.0 psu below Bass Strait (which is commonly the case). Then the rate of increase in salinity due to flushing in the model is $\frac{1}{270}$ per day, whereas in reality it should be something like $\frac{1}{340}$ per day. The difference between these rates amounts to 0.00076 (psu) per day. This can be converted to an equivalent evaporation rate of about 0.3mm per day, which is close to 8% of the long term evaporation rate (about 1400mm/year, or almost 4mm/day). So, it should be possible to grossly compensate the shorter model flushing time in this situation by decreasing evaporation by about 8%. However, as shown above, a 30% decrease is needed to produce realistic model salinities. The shorter flushing time could still account for this if the salinity in the bulk of the Bay was consistently 4 psu below the salinity in Bass Strait, but this is certainly not the case. In fact, even during periods when the Bay salinity is near or above that of Bass Strait, the model still consistently overestimates salinity. This cannot be caused by exchange with Bass Strait, which cannot raise salinity above a value of about 35.4.

Alternatively, the problem may lie with the evaporation or freshwater input data. As demonstrated above, grossly similar changes in model output can be achieved by altering either one in the appropriate manner. However, their effects are not entirely inseparable. For example, their time histories are different, so that large and sudden decreases in salinity in the Bay, as observed in late 1992 and late 1993, must be due to freshwater input events (direct rainfall on the Bay, flood inputs, or most likely some combination of both). As well, the spatial distributions of evaporation, rainfall and point source inputs are different, so that altering any one may change the response from site to site in different ways. At the time of writing this report, investigations of these aspects were underway, and some inverse modelling had been done in order to better quantify the freshwater budget for the Bay, but these tasks were not complete. However, given that the model performance can be dramatically improved by a simple scaling of inputs, the overall conclusion that can be drawn is that there is a systematic bias either in the observed inputs of fresh-water into the Bay (which must currently be underestimated), or in the evaporation from the Bay (which must currently be overestimated), or most likely some combination of both.

For the purposes of assessing how well the model simulates salinity values over both time and space, this systematic error was reduced by a somewhat arbitrary decision to scale input rainfall by a factor of 1.6. This is a large change, equivalent to increasing the long term rainfall rate from about 650mm/year to 1040mm/year. Alternatively, it is equivalent to increasing the surface area of the Bay by a factor of 1.6, or adding all the rain which falls on a coastal strip about 5km wide surrounding the Bay. As discussed above, similar results could be obtained by scaling evaporation by a factor of 0.7 (reducing it to a value of about 1000mm/year). Note that none of these alternatives is proposed here as the definitive answer to the fresh water budget problem, and the correct solution is probably some combination of all of these effects.

Simulations of salinity were performed for the 59 box model with 1 water column layer (runs were also done with up to 5 layers in the vertical, with essentially identical results). The resulting salinity time series at each site are discussed in detail below.

4.3.1 Site 1

Figure 18 shows measured and modelled salinity at site 1 (box 3 in the model), which is located near Blairgowrie in the far south of the Bay. The modelled and observed salinity at this site show fair agreement (slope = 0.47, $r^2 = 0.67$), with the model tending to show less seasonal variability than is observed. This is likely to be due to the location of Site 1, so that the model has only 2 boxes between site 1 and Bass Strait. As a result, the model exchanges water between this site and Bass Strait somewhat faster than the exchange which occurs in reality (see Figure 13), and the modelled salinity at this site tends to stay closer to the salinity of Bass Strait.

4.3.2 Site 4

Figure 19 shows measured and modelled salinity at site 4 (box 17 in the model), which is located near Wooley Reef in the south-east of the Bay. There is reasonably good agreement between the model and observations at this site. When all data is used, an r^2 value of 0.65 and slope of 0.58 is obtained, but this improves to 0.79 and 0.70 respectively if the single point where observed salinity is less than 30 is omitted. Sudden low salinity 'spikes' are seen in both the model and observations, due to fresh-water inputs from both the Yarra River and the Patterson River/Mordialloc Creek system. These are discussed further for Sites 6 and 9 below, where they are even more pronounced.

4.3.3 Site 6

Figure 20 shows measured and modelled salinity at site 6 (box 29 in the model), which is located near Sandringham on the eastern side of the Bay. In both the model results and observations, this site shows sharp low salinity spikes which are caused by large flow events in the Yarra river, and the resultant plume of fresher water extending down the eastern side of the Bay. The model shows good agreement with observations at salinities above 30 (which accounts for all but 4 of the data points, slope = 0.74, $r^2 = 0.71$), but does not reproduce the lowest salinity spikes well. This is due to model resolution - the model salinity represents a uniform value over a box which has an area of about 23 square kilometres, whereas the observation is a point measurement. During times of large freshwater input, there will be large spatial gradients in salinity across the plume extending down the coast, so that the observed value will be sensitive to the measurement location. The limited resolution of the model smears these spatial gradients.

4.3.4 Site 9

Figure 21 shows measured and modelled salinity at site 9 (box 32 in the model), which is located in Hobsons Bay near the mouth of the Yarra River. As expected, this site shows the most variability in salinity of any site in the Bay, due to its proximity to the mouth of the Yarra River. The model is again limited by its spatial resolution, doing a fair job of reproducing observed salinities (slope = 0.38, $r^2 = 0.54$ for all data, and slope = 0.68, $r^2 = 0.47$ for observed salinity greater than 30). Box 32 covers an area of about 49 square kilometres, including most of Hobsons Bay. As a result, the model is again unable to reproduce the very strong spatial gradients in salinity in the vicinity of this site. Nevertheless, the overall seasonal variation in salinity, and qualitative characteristics of this site are well reproduced.

4.3.5 Site 11

Figure 22 shows measured and modelled salinity at site 11, (box 49 in the model), which is located near the Werribee River in the north-west of the Bay. The model does a good job of representing salinity at this site (slope = 1.01, $r^2 = 0.75$). There is a single modelled low salinity spike in late 1993 which is not seen to the same extent in the observations. This is most probably due to a short-lived but high flow flood in the Werribee River, described in Walker 1997 (Technical Report 38).

4.3.6 Site 13

Figure 23 shows measured and modelled salinity at site 13 (box 38 in the model), which is located in the Geelong arm. The model does a good job of representing salinity at this site (slope = 0.89, $r^2 = 0.87$), although it yields values which are on average about 0.27 psu low. This site shows the highest salinities in the Bay - it is remote from the major river inputs to the Bay, and also exhibits a longer than average flushing time with respect to Bass Strait.

4.3.7 Site MW1

Figure 24 shows measured and modelled salinity at site MW1 (box 53 in the model), which is located towards the southern side of the main body of the Bay (north of the Great Sands). The model does a good job of representing salinity at this site (slope = 0.94, $r^2 = 0.89$), although it generally yields values which are a little high (about 0.17 psu on average). Observations available at this site only covered the period from 19 January 1993 to 27 March 1995.

4.3.8 Site MW2

Figure 25 shows measured and modelled salinity at site MW2 (box 59 in the model), which is located in the centre of the Bay. The model does a very good job of representing salinity at this site (slope = 0.99, $r^2 = 0.91$). Again, available observations at this site only covered the period from 19 January 1993 to 29 March 1995.

Several other sites which were sampled as part of the study were not included in the above comparisons due to the short period over which observational data was available. In general, the above comparisons show that the model reproduces well both the temporal and spatial variations of salinity in the Bay. Salinity is highly variable near major river inputs, and has a more obvious seasonal and inter-annual variation elsewhere in the Bay. The main issue which needs to be resolved in order to give these comparisons the status of a rigorous model validation is the necessity for a significant correction to be applied to the freshwater budget.

4.4 Sediments

At the time of writing this report, realistic simulations of the transport of inorganic particulates have not been performed. Issues here include the characterisation of particulate inputs to the Bay, the initialisation of model sediment layers from the task P7 core sample data, the vertical resolution of the model, and the detailed analysis of task P7 SEDCAM data in order to provide validation data sets. As far as ecological simulations are concerned, the main impact of the lack of realistic inorganic sediment transport in the model is that their effect on light attenuation cannot be modelled. Light attenuation is discussed further in Murray and Parslow 1997 (Technical Report 44).

5 Conclusion

A Transport Model has been developed which includes the major physical processes which move dissolved and particulate substances in the water column and between the water and sediments. This model has been implemented for Port Phillip Bay at various resolutions, with most effort concentrated on a model which represents the Bay with 59 boxes. The model is coupled to a Hydrodynamic Model to obtain water movements, and Hydrodynamic Model output is currently available to drive the model for the period from July 1990 to June 1995.

Model validation in the water column has been performed by simulating salinity. This exercise identified significant systematic biases in the fresh-water inputs to the model. The 59 box model flushes in about 270 days, compared to an estimated value for the Bay of about 340 days. The salinity comparisons using scaled fresh water inputs show that the model is capable of doing a good job of representing salinity variations in both space and time. The most appropriate way in which to modify the fresh-water budget of the Bay is an unresolved issue at the time of writing, and it deserves further investigation. Validation of the sediment portion of the model, particularly the transport of inorganic particulates, is incomplete. Again, this deserves further attention.

The model has been used as the physical framework for the ecological modelling efforts carried out during the study. These efforts are described in Murray and Parslow 1997 (Technical Report 44).

6 Acknowledgements

Many people and organisations contributed to the development of the model and data sets described in this report. Data sets were obtained from the Victorian EPA, the Bureau of Meteorology, Melbourne Water, VFRI and VIMS (now MAFRI), the University of Western Australia, and Lawson and Treloar Pty. Ltd. Model development was aided by valuable discussions with and input from John Hunter, John Parslow, Sandy Murray and Jason Waring. Brian Newell, Colin Arrowsmith, Doug Hall and Rob Molloy provided valuable support and interfacing throughout the study.

Funding was provided by Melbourne Water through the Port Phillip Bay Environmental Study.

References

Beasley, A. W., 1966: Port Phillip survey 1957–1963. bottom sediments, *Mem. Nat. Mus. Vic.*, 27, 69–105.

Beer, T., F. Carnovale, C. Carvalho and M. E. Cope, 1992: Literature review of the physica and chemical atmospheric inputs to Port Phillip Bay, *Tech. Rep. 5,* CSIRO Port Phillip Environmental Study.

Blackburn, N. D., and T. H. Blackburn, 1993: A reaction diffusion model of C-N-S-O species in a stratified sediment, *FEMS Microbiology Ecology, 102,* 207–215.

(CERC), C. E. R. C., 1988: *Shore protection manual, U. S.* Army corps of engineers.

Delo, E. A., 1988: Estuarine muds manual, *Tech. Rep. SR164,* Hydraul. Research, Wallingford, England .

Glenn, S. M., and W. D. Grant, 1987: A suspended sediment stratification correction for combined wave and current flows, J. *Geophys. Res.,* 92(C8), 8244–8264.

Grant, W. D., and O. S. Madsen, 1982: Movable bed roughness in unsteady oscillatory flow, J. *Geophys. Res.*, 87, 469–481.

Greilach, P., Z. You, K. Black and R. gorman, 1996: Sediment characteristics in Port Phillip Bay, *Tech. Rep. 23,* CSIRO Port Phillip Bay Environmental Study.

Hamblin, P. F., 1989: Observations and model of sediment transport near the turbidity maximum of the upper Saint Lawrence Estuary, J. *Geophys. Res., 94(C10),* 14419–14428.

Harris, G., G. Batley, D. Fox, D. Hall, P. Jernakoff, R. Molloy, A. Murray, B. Newell, J. Parslow, G. Skyring and S. Walker, 1996: Port Phillip Bay Environmental Study final report, *Tech. rep.,* CSIRO.

Hunter, J. R., 1992: Review of physical processes, in *Port Phillip Pay Environmental Study: Status reDiew,* edited by D. N. Hall, Technical Report 9, CSIRO.

Komar, P. D., 1976: *Beach processes and sedimentation,* Prentice-Hall.

Lavelle, J. W., H. O. Mofjeld and E. T. Baker, 1984: An in situ erosion rate for a fine "rained marine sediment, J. *Geophys. Res.*, 89(C4), 6543–6552.

Luettich, Jr., R. A., D. R. F. Harleman and L. Somlyódy, 1990: Dynamic behavior of suspended sediment concentrations in a shallow lake perturbed by episodic wind events, *Limnology and Oceanography, pp.* 1050–1067.

Madsen, O. S., 1994: Spectral wave-current bottom boundary layer flows, in *Coastal engineering 1994 Proceedings, 24th international conference Coastal Engineering Research Council/A SCE.*

McLean, S. R., 1992: On the calculation of suspended loads for noncohesive sediments, J. *Geophys. Res.,* 97(C4), 5759–5770.

MMBW/FWD, 1973: Environmental study of Port Phillip Bay: Report on Phase One 1968-1971, *Tech. rep.,* Melbourne and Metropolitan Board of Works and Fisheries and Wildlife Department of Victoria.

Murray, A. G.. and J. P. Parslow, 1997: Port Phillip Bay integrated model: final report, *Tech. Rep. 44,* CSIRO Port Phillip Bay Environmental Study.

Nittrouer, C. A., and L. D. Wright, 1994: Transport of particles across continental shelves, *Rev. Geophys., 32(1),* 85–113.

NSR Environmental Consultants Pty Ltd. 1993: Surface inputs into Port Phillip Bay (excluding the Yarra river and WTC), *Tech. Rep. 12,* CSIRO PPBES.

Pattiaratchi, C., R. Phillips, C. Oldham and A. Perkins, 1996: Mixing, flushing and ctd surveys of the waters of Port Phillip *Bay, Tech. Rep. 34,* CSIRO Port Phillip Bay Environmental Study.

Sheng, Y. P., and C. Villaret, 1989: Modeling the effect of suspended sediment stratification on bottom exchange processes, J. *Geophys. Res.,* 94(C10), 14429–14444.

Sherwood, C. R., 1995: Measurements and modeling of suspended sediment transport on the northern California continental shelf, Ph.D. thesis, University of Washington.

Smith, J. D., 1970: Modeling of sediment transport on continental shelves, in *The Sea,* edited by E. D. Goldberg, I. N. McCave, J. J. O, Brien, and J. H. Steele, number 6, pp.539–577, Wiley-Interscience.

Smith, J. D., and S. R. McLean, 1977: Spatially averaged flow over a wavy surface, J. *Geophys. Res.,* 82, 1735–1746.

Teisson, C., 1991: Cohesive suspended sediment transport: feasibility and limitations of numerical modelling, J. *Hydraul. Res., 29,* 755–768.

Uncles, R. J., and J. A. Stephens, 1989: Distributions of suspended sediment at high water in a macrotidal estuary, J. *Geophys. Res.,* 94(C10), 14395–14405.

Walker, S. J., 1997: Hydrodynamic models of Port Phillip Bay, *Tech. Rep. 38,* CSIRO Port Phillip Bay Environmental Study.

White, S. J., 1970: Plane thresholds of fine "rained sediments, *Nature,* 228, 152–153.

Wiberg, P. L., D. E. Drake and D. A. Cacchione, 1994: Sediment resuspension and bed armoring during high bottom stress events on the northern California inner continental shelf: Measurements and predictions, *Continental Shelf Research,* 14, 1191–1219.

Wiberg, P. L., and C. K. Harris, 1994: Ripple geometry in wave dominated environments, J. *Geophys. Res., 99,* 775–789.

Wiberg, P. L., and D. M. Rubin, 1989: Bed roughness produced by saltating sediment, J. *Geophys. Res.,* 94, 5011–5016.

List of Figures

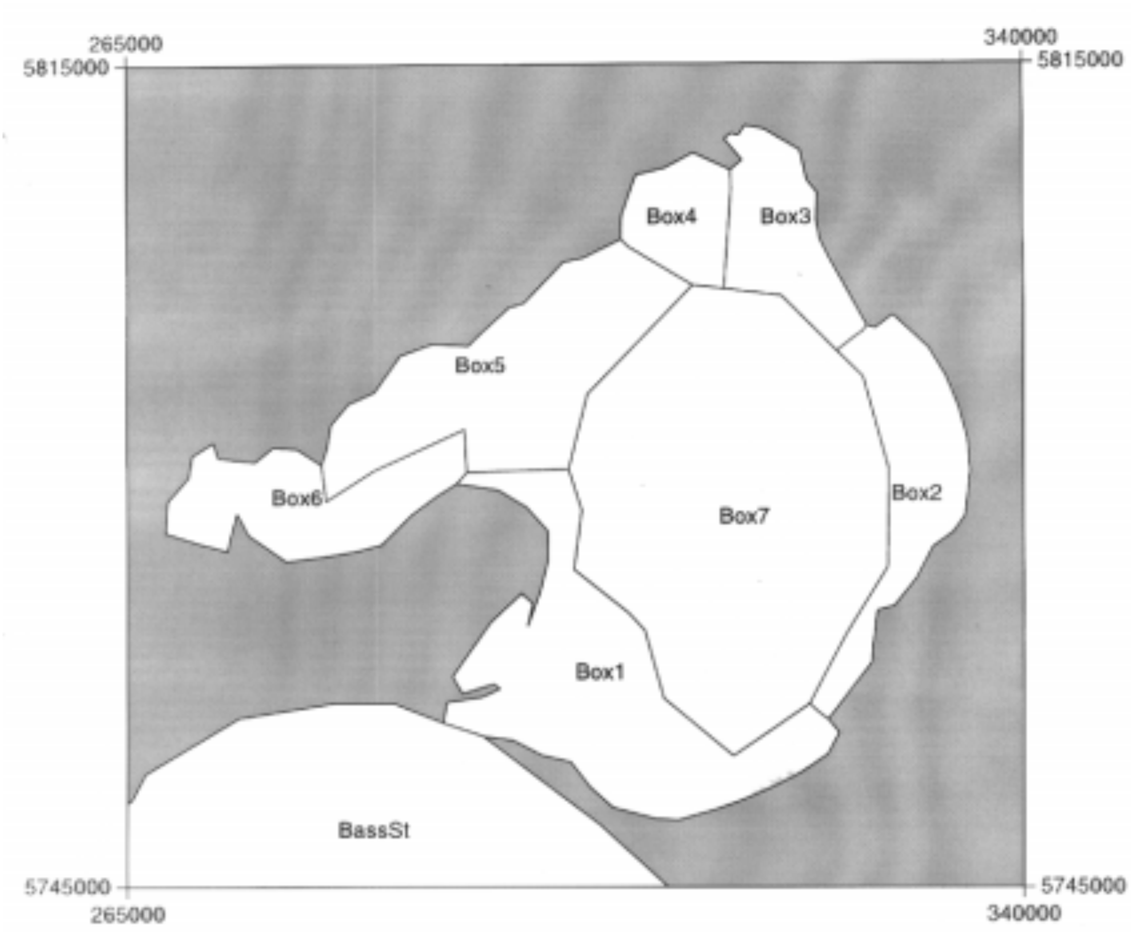

Figure 1: Seven-box model of Port PhillipBay. The box boundaries for this model were chosen primarily on the basis of the regions identified in the Phase One study report (MMBW/FWD 1973). Coordinates on this and other geographic plots are in meters (AMG, Zone 55).

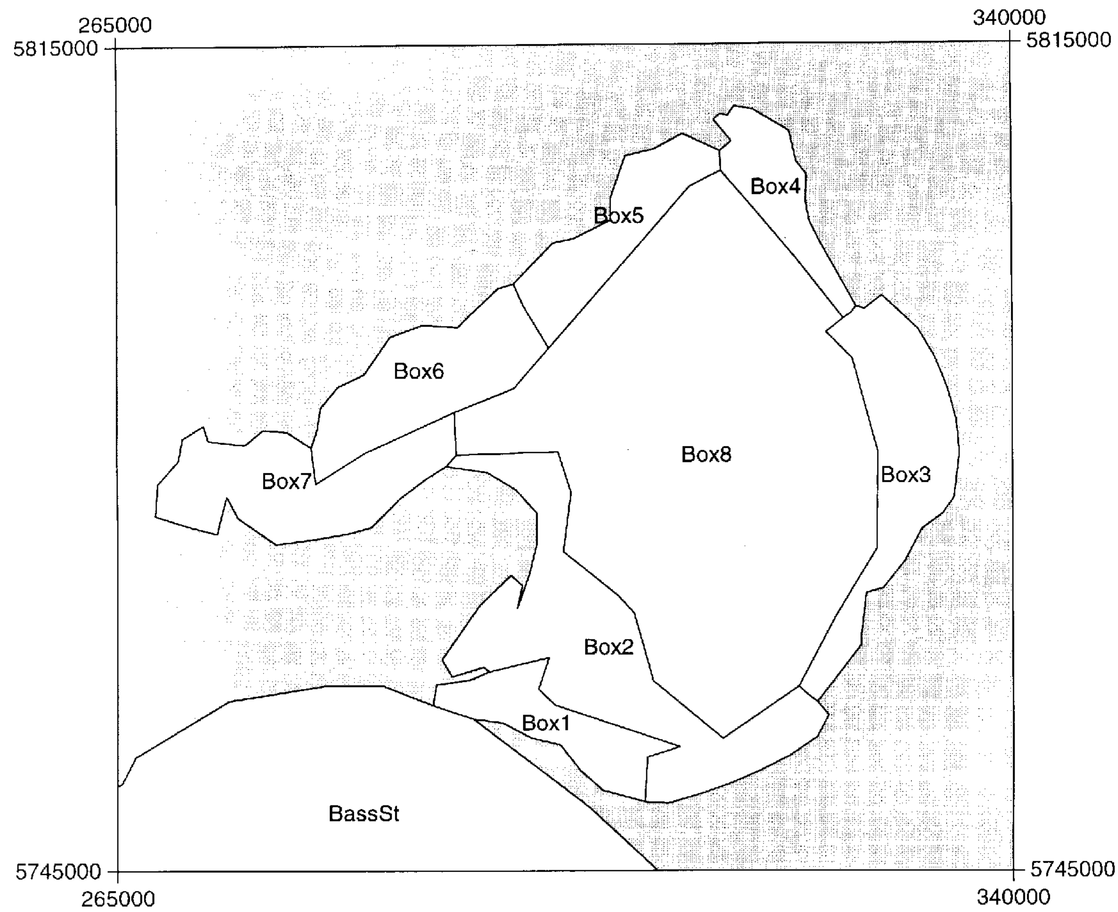

Figure 2: Eight-box model of Port Phillip Bay. This model evolved from the seven-box model, with the coastal boxes made narrower, and an extra box inserted to the south of the Great Sands to improve the flushing characteristics of the model.

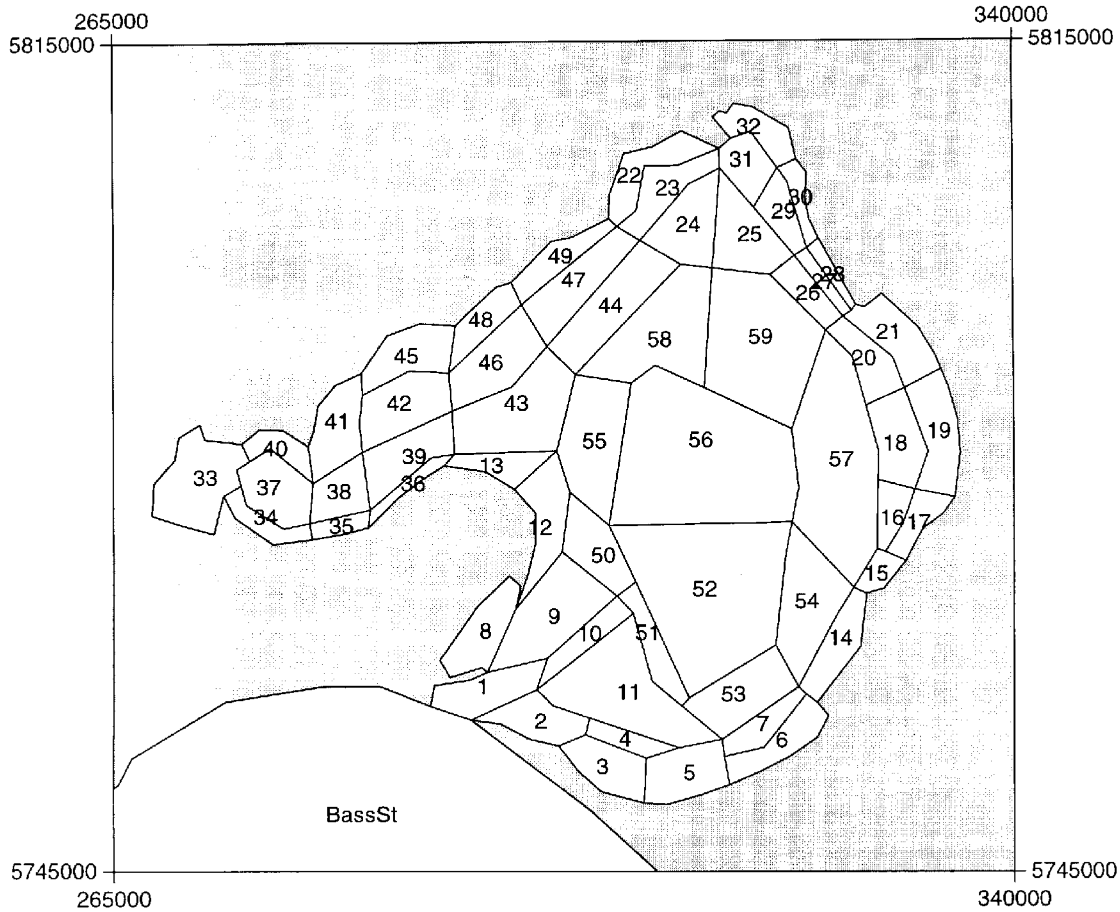

Figure 3: Fifty nine-box model of Port Phillip Bay. The box boundaries in this model were loosely based on the 5, 10, 15 and 20 metre depth contours, with further radial sub-divisions based on the distributions of point inputs and locations of various areas of interest. The boxes in the 1, 6, 7 and 8-box models are made by joining boxes from the 59 box model together.

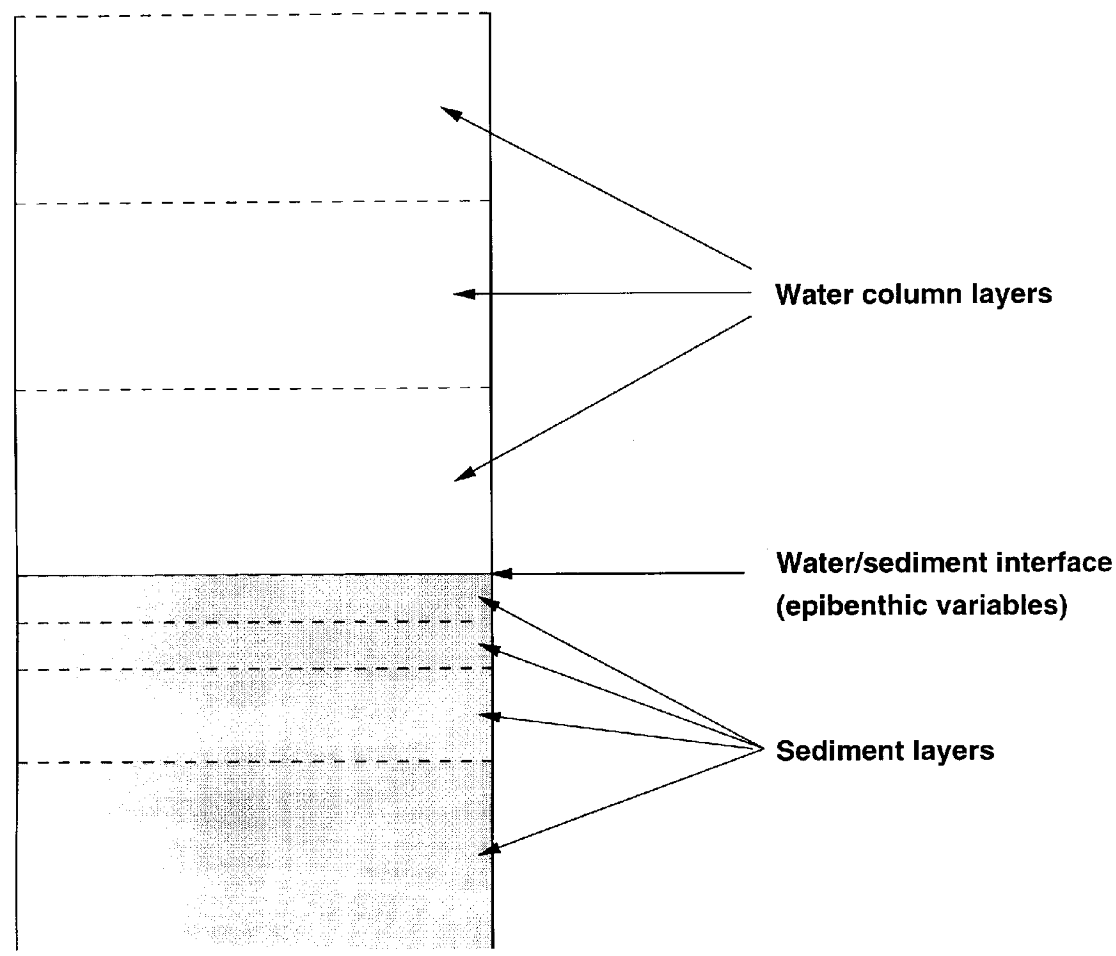

Figure 4: Vertical structure of a single Transport Model box.

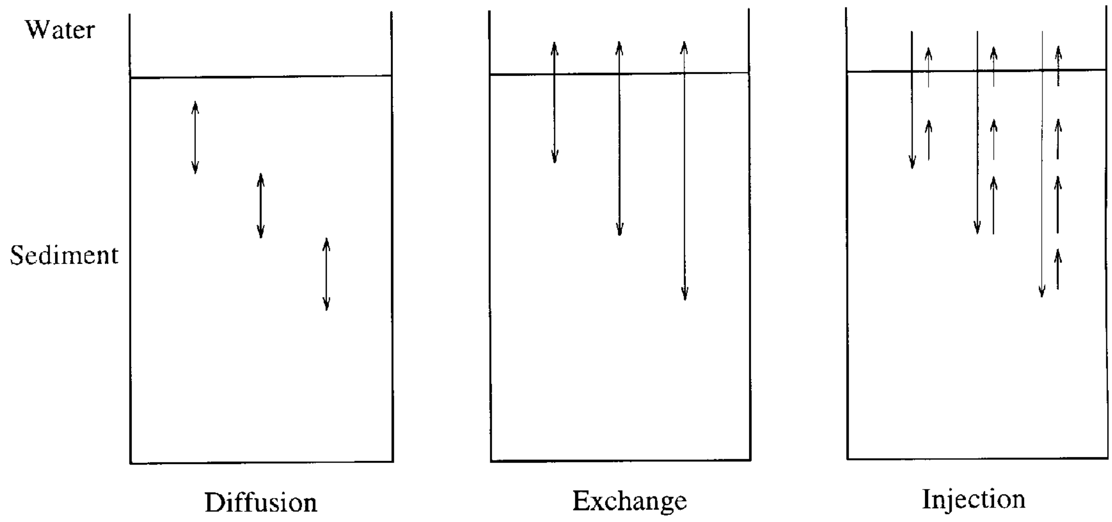

Figure 5: Schematic diagram of bioirrigation processes represented in the Transport Model.

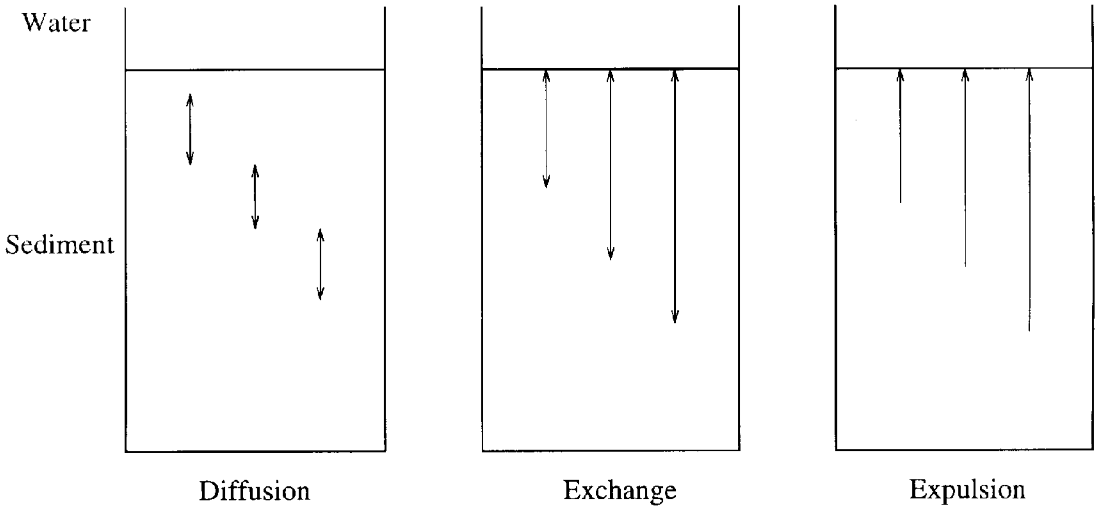

Figure 6: Schematic diagram of bioturbation processes represented in the Transport Model.

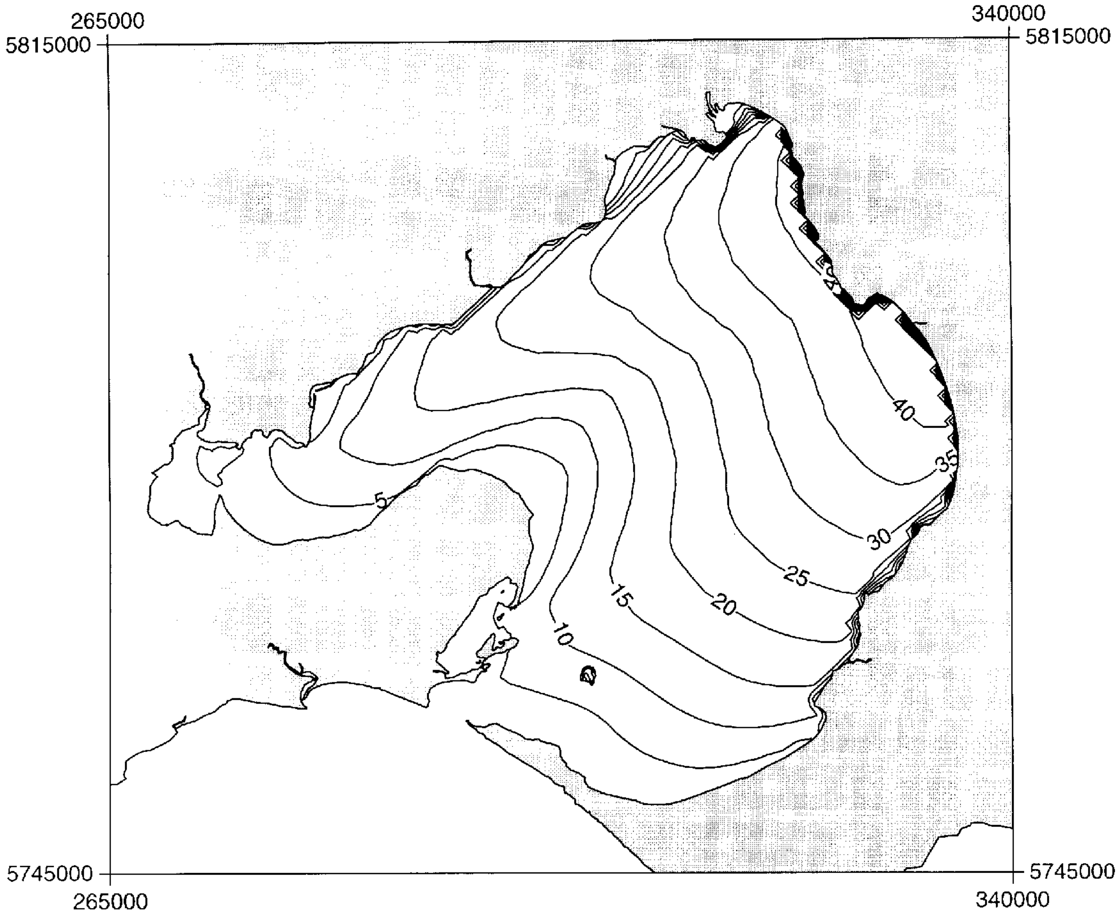

Figure 7: Fetch contours (km) for wind from 230° (the mean wind direction for about the 8 hours prior to 1600, 19 September 1994).

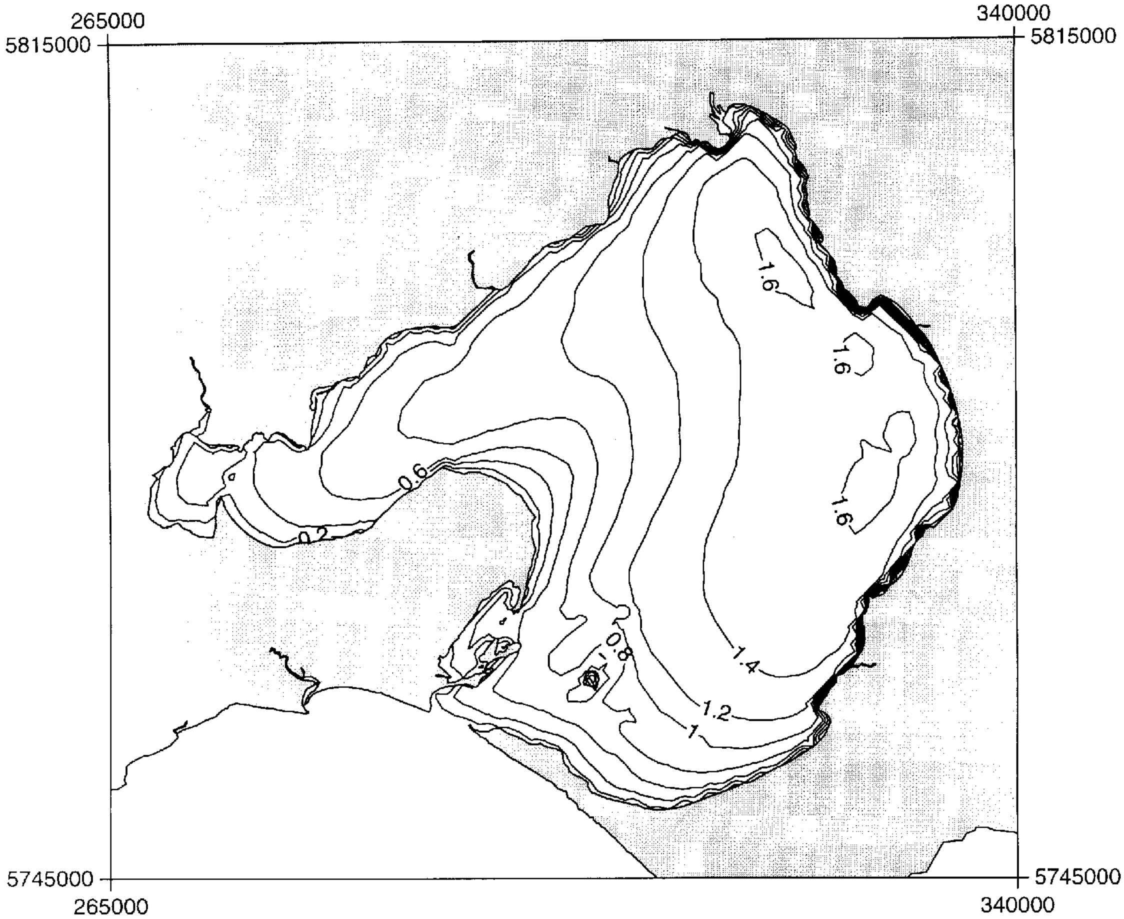

Figure 8: Contours of sign)ficant wave height (m) calculated at 1600, 19 September 1994, during strong south westerly winds.

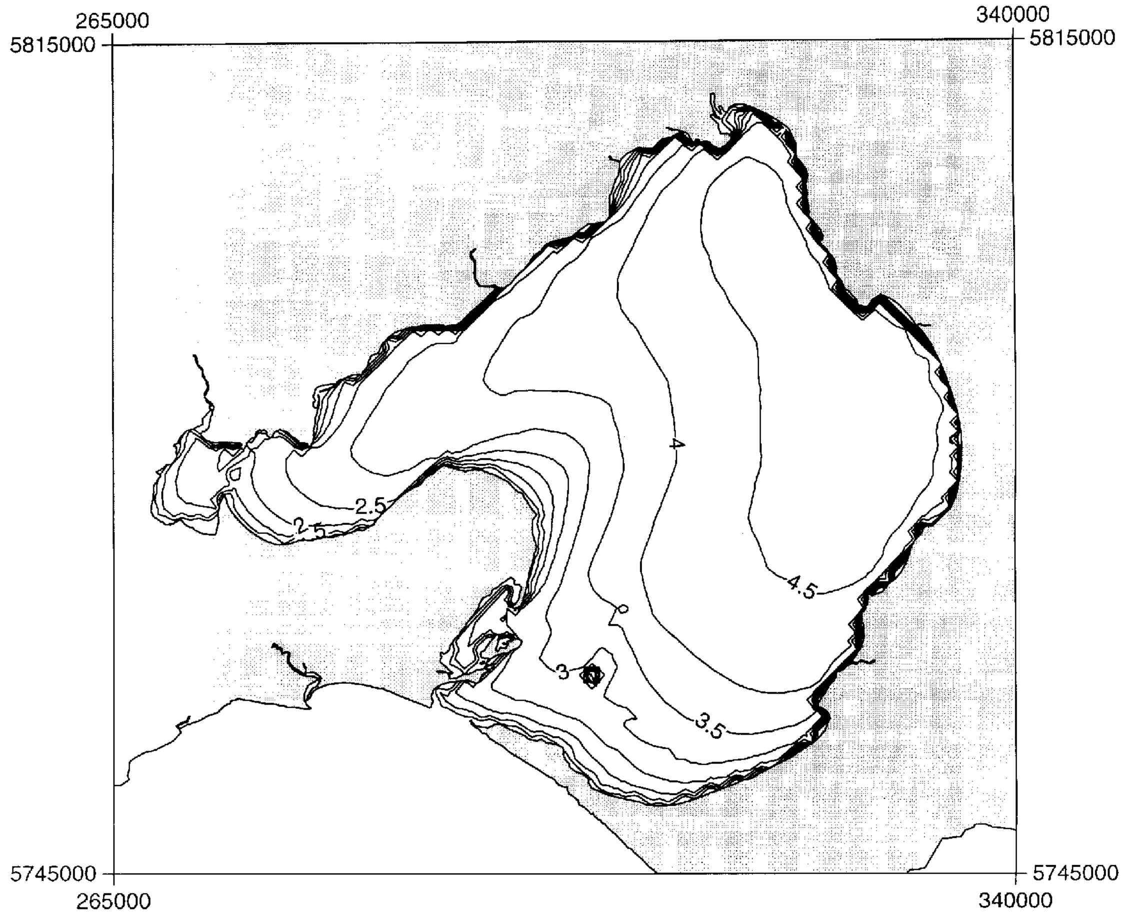

Figure 9: Contours of dominant wave period (s) calculated at 1600, 19 September 1994, during strong south westerly winds.

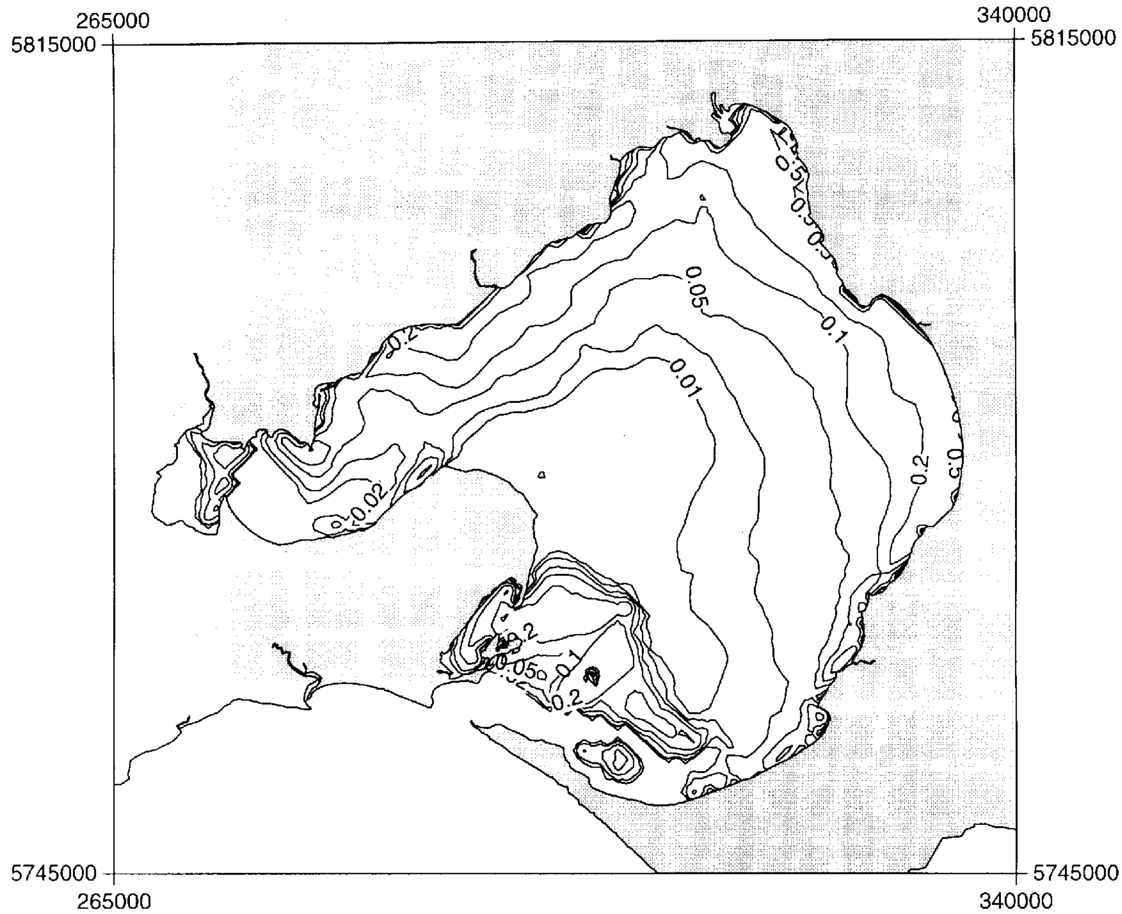

Figure 10: Contours of bottom orbital velocity (m/s) calculated at 1600, 19 September 1994, during strong south westerly winds.

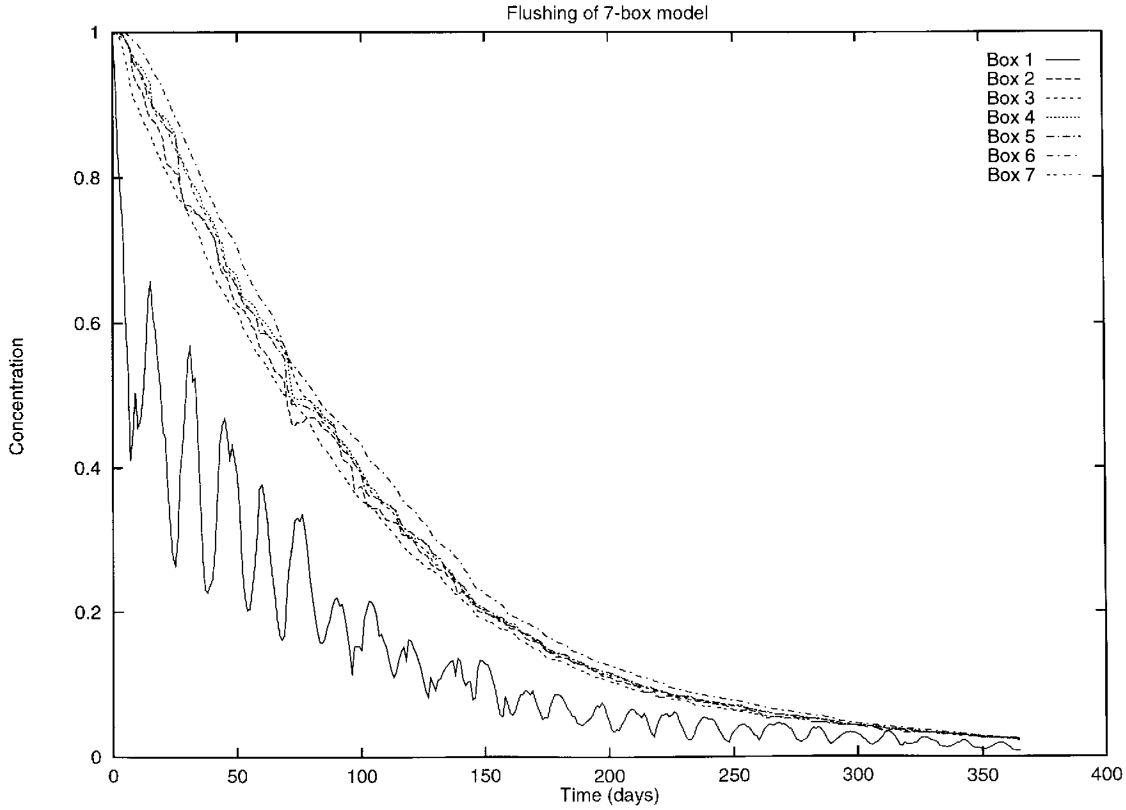

Figure 11: Simulated flushing for the 7-box Transport Model. The tracer has an initial concentration of 1 everywhere in the Bay and 0 in Bass Strait.

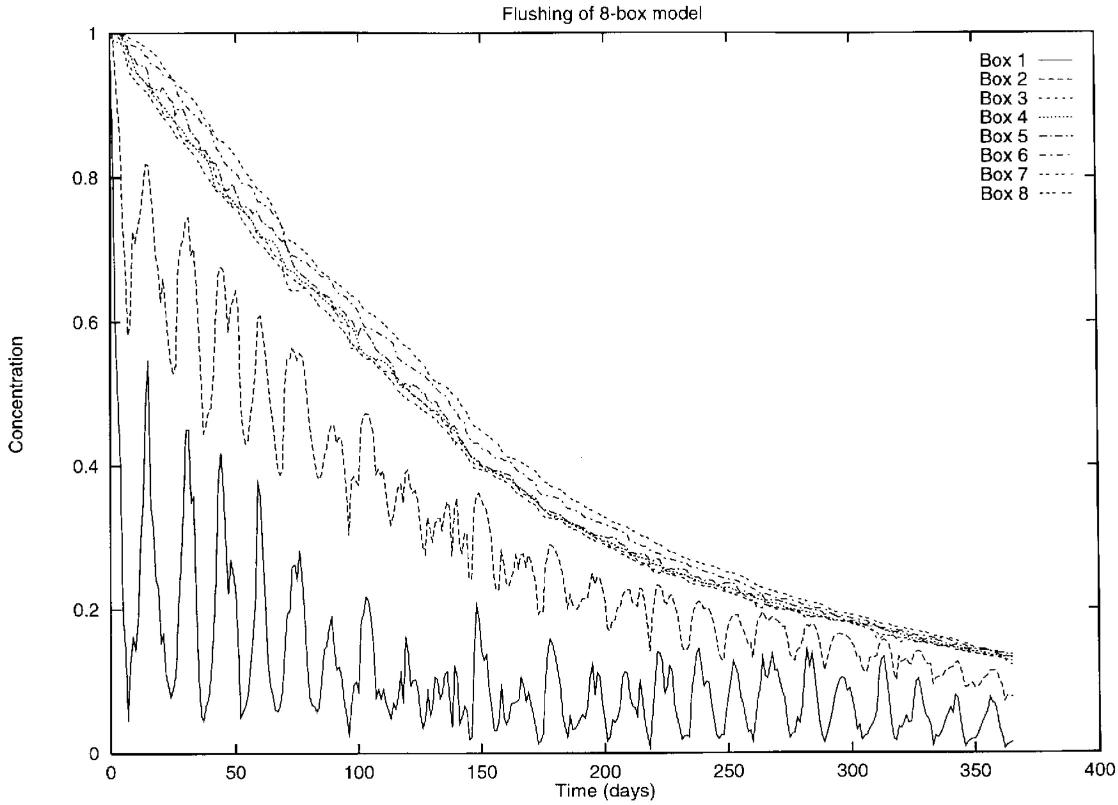

Figure 12: Simulated flushing for the 8-box Transport Model. The tracer has an initial concentration of 1 everywhere in the Bay and 0 in Bass Strait.

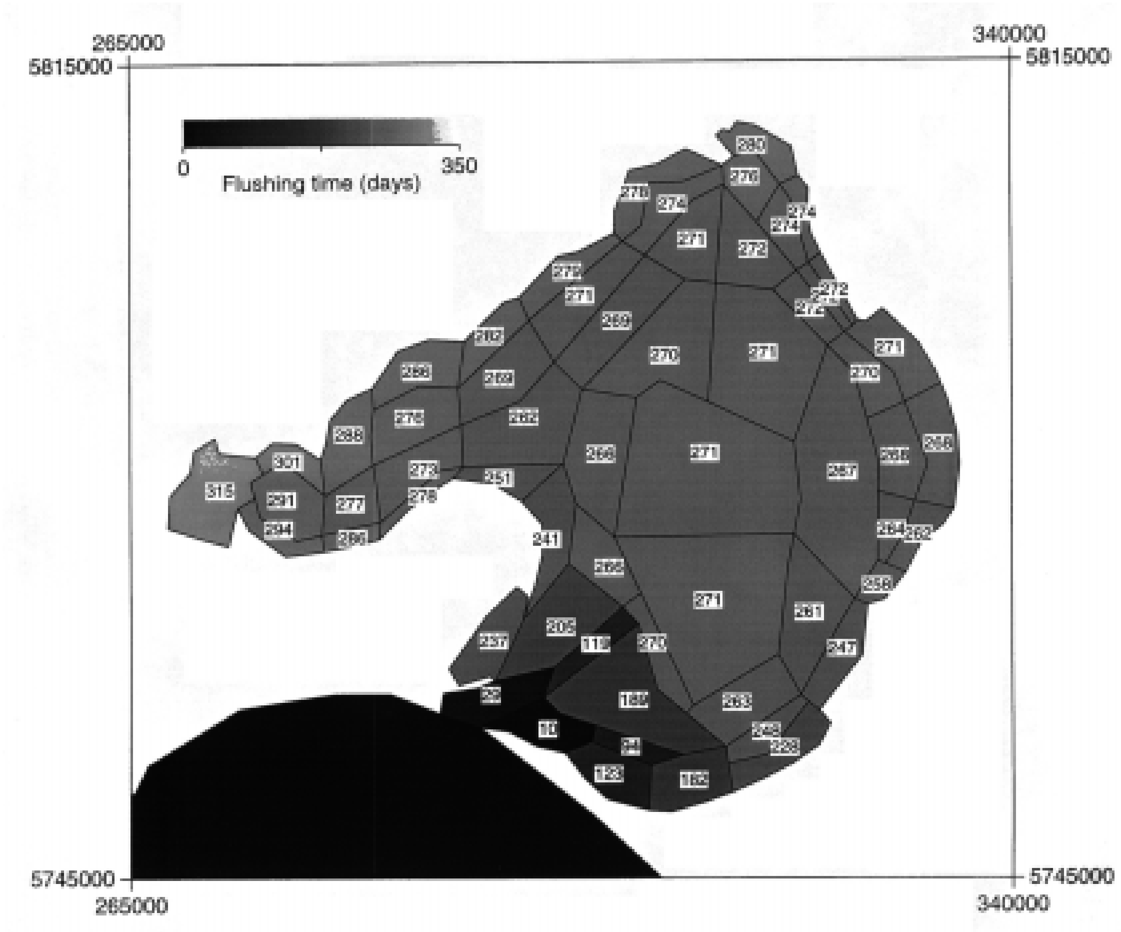

Figure 13: Simulated flushing for the 59-box Transport Model. Flushing times for each box were calculated from concentration time series for a tracer which had an initial concentration of 1 everywhere in the Bay and 0 in Bass Strait.

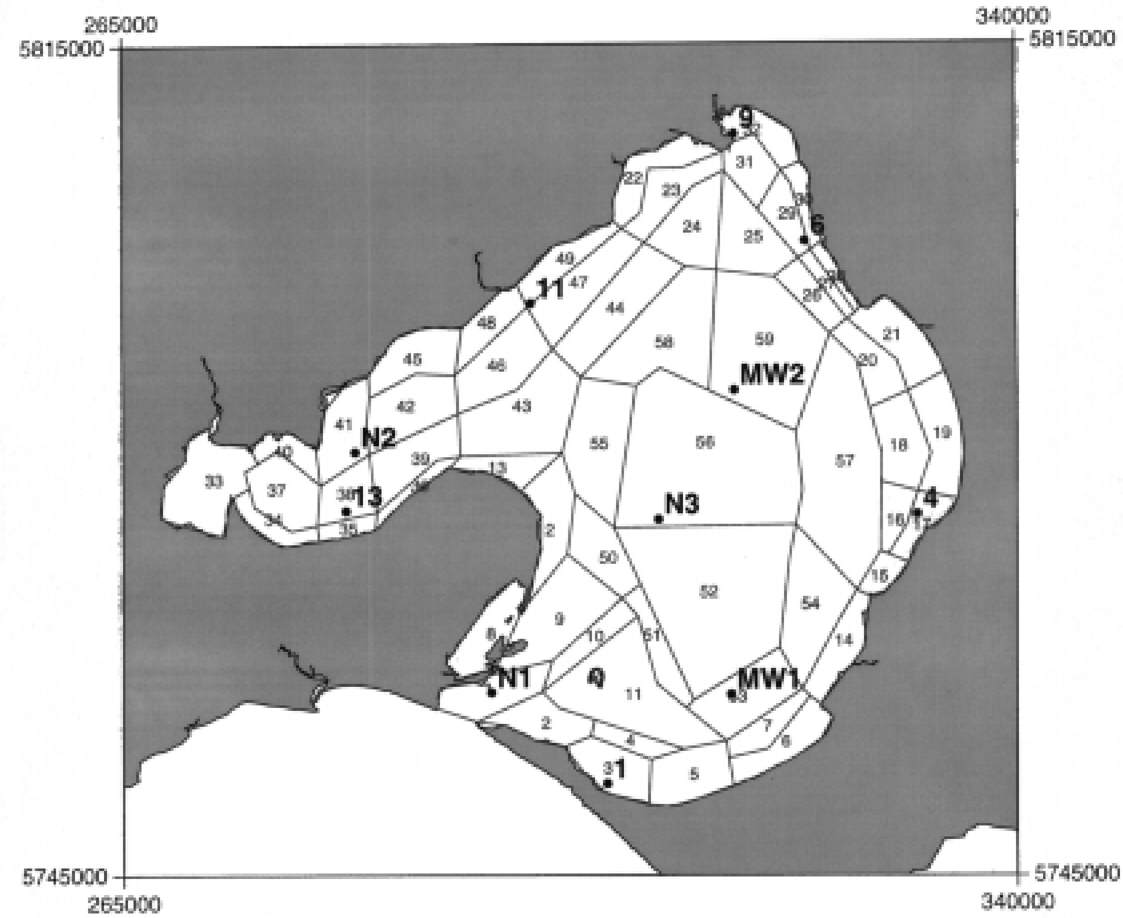

Figure 14: Locations of VFRI sampling sites 1, 4, 6, 9, 11, 13, MW1, MW2, N1, N2 and N3.

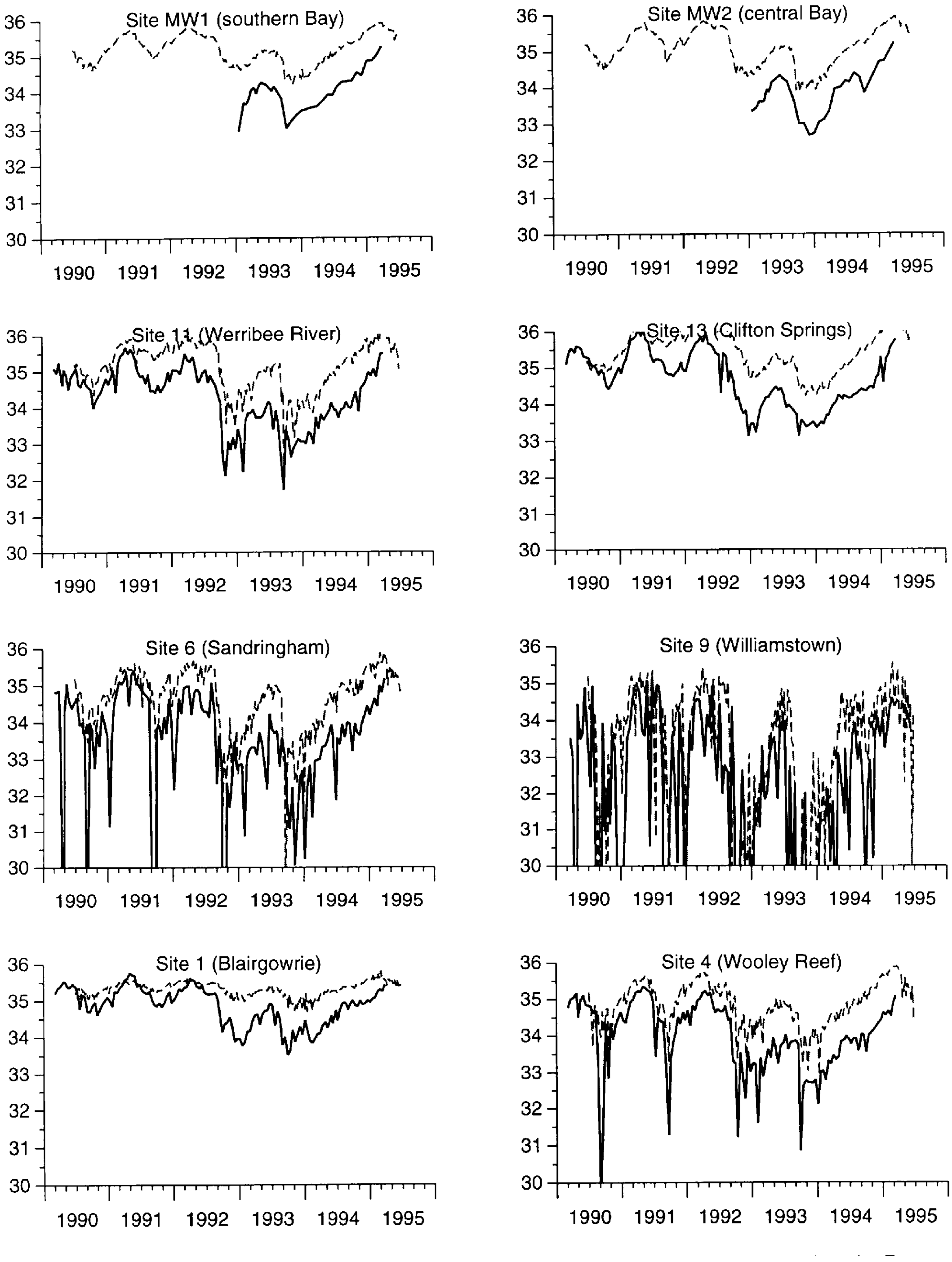

Figure 15: Measured (solid line) and modelled (dashed line) salinities at 8 sites in Port Phillip Bay, over the period 1990 to 1995. For this simulation, freshwater inputs were as obtained by the study.

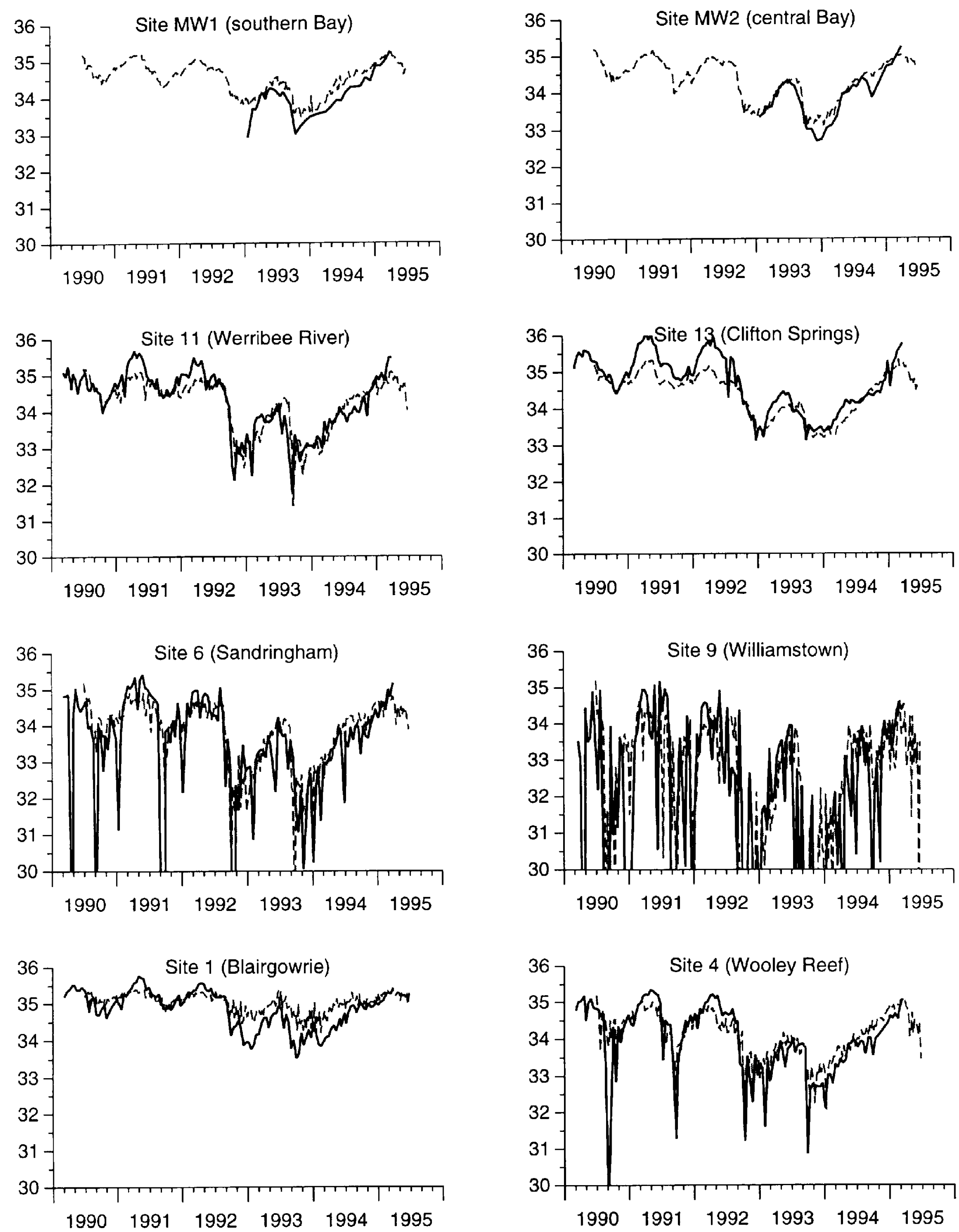

Figure 16: Measured (solid line) and modelled (dashed line) salinities at 8 sites in Port Phillip Bay, over the period 1990 to 1995. For this simulation, evaporation inputs were scaled by a factor of 0.7.

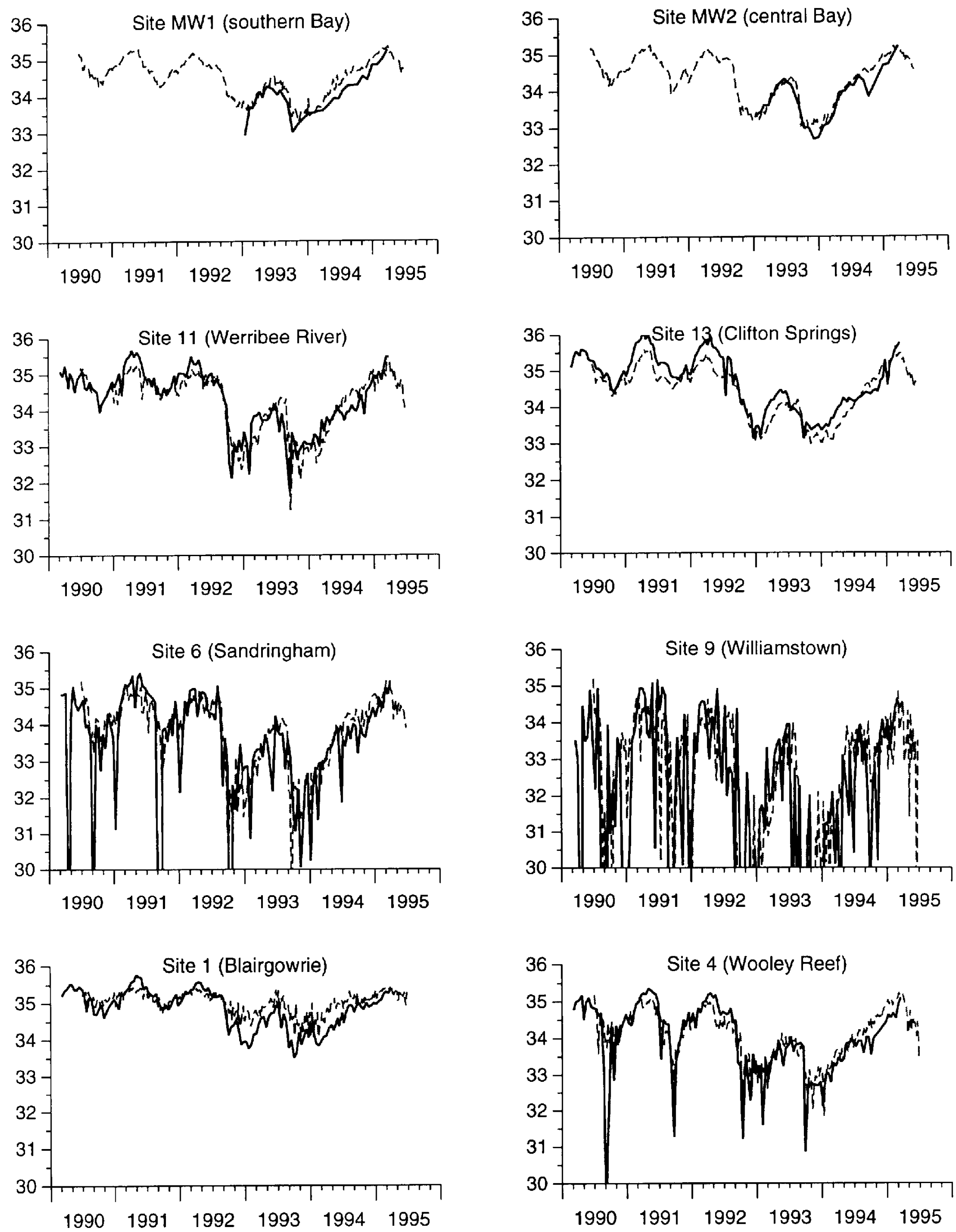

Figure 17: Measured (solid line) and modelled (dashed line) salinities at 8 sites in Port Phillip Bay, over the period 1990 to 1995. For this simulation, rainfall inputs were scaled by a factor of 1.6.

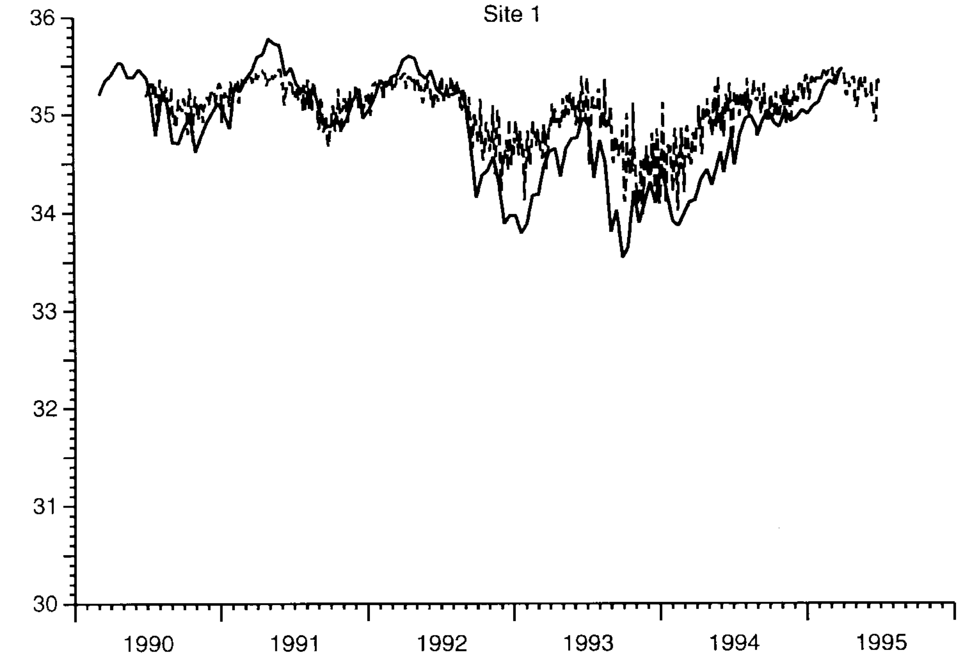

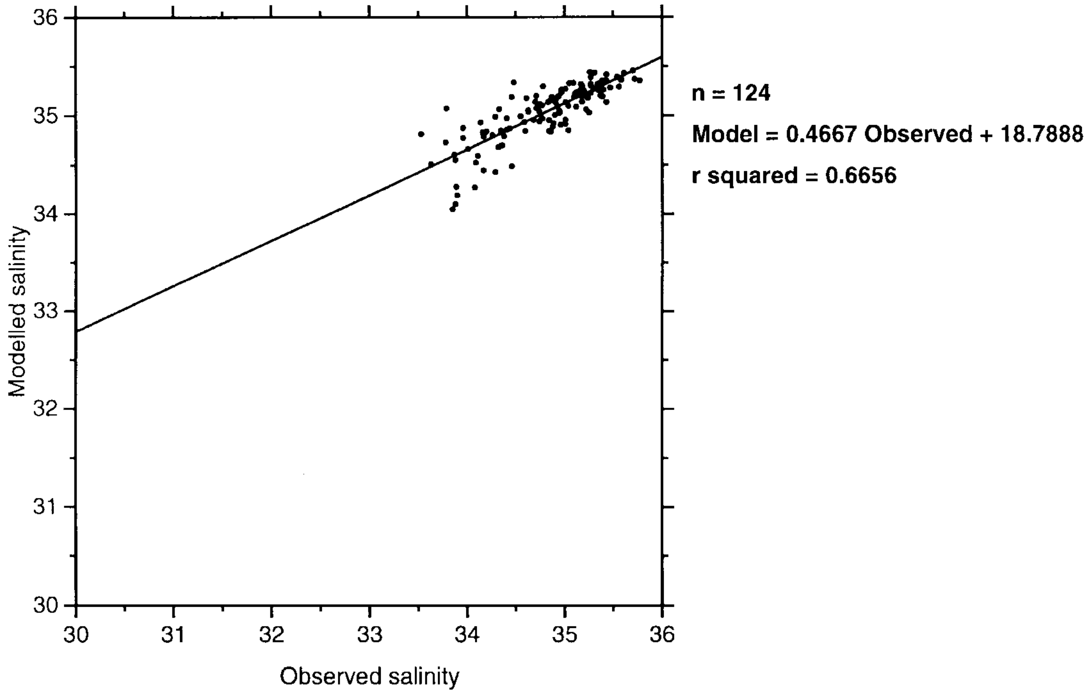

Figure 18: The upper plot shows time series of measured (solid line) and modelled (dashed line) salinities at Site 1 over the period 1990 to 1995. For this simulation, rainfall inputs were scaled by a factor of 1.6. The lower plot shows a scatter plot of these salinity data, together with linear regression values and line of best fit.

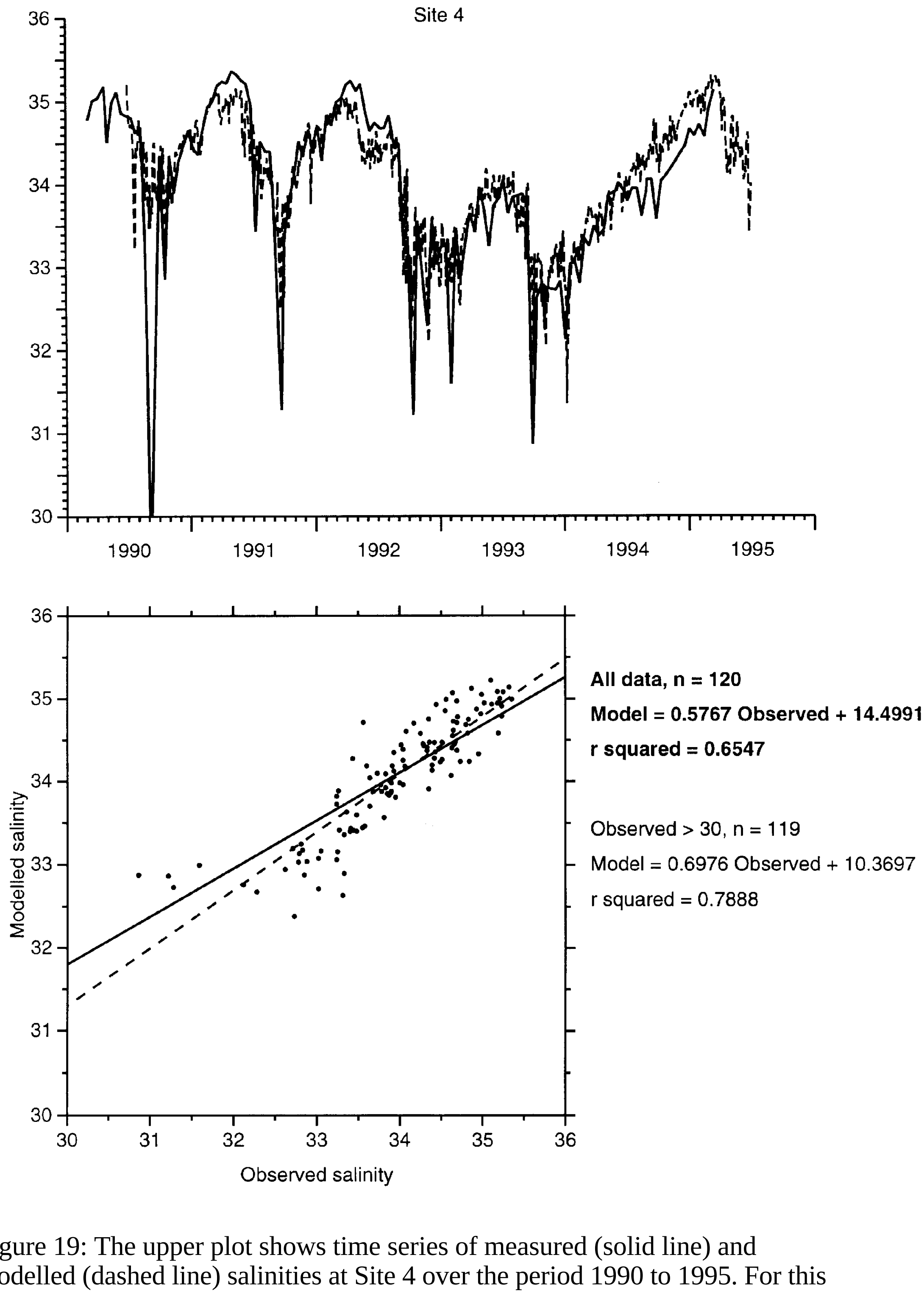

Figure 19: The upper plot shows time series of measured (solid line) and modelled (dashed line) salinities at Site 4 over the period 1990 to 1995. For this simulation, rainfall inputs were scaled by a factor of 1.6. The lower plot shows a scatter plot of these salinity data, together with linear regression values and lines of best fit for both all data (solid line and bold text) and for measured values greater than or equal to 30 (dashed line and normal text).

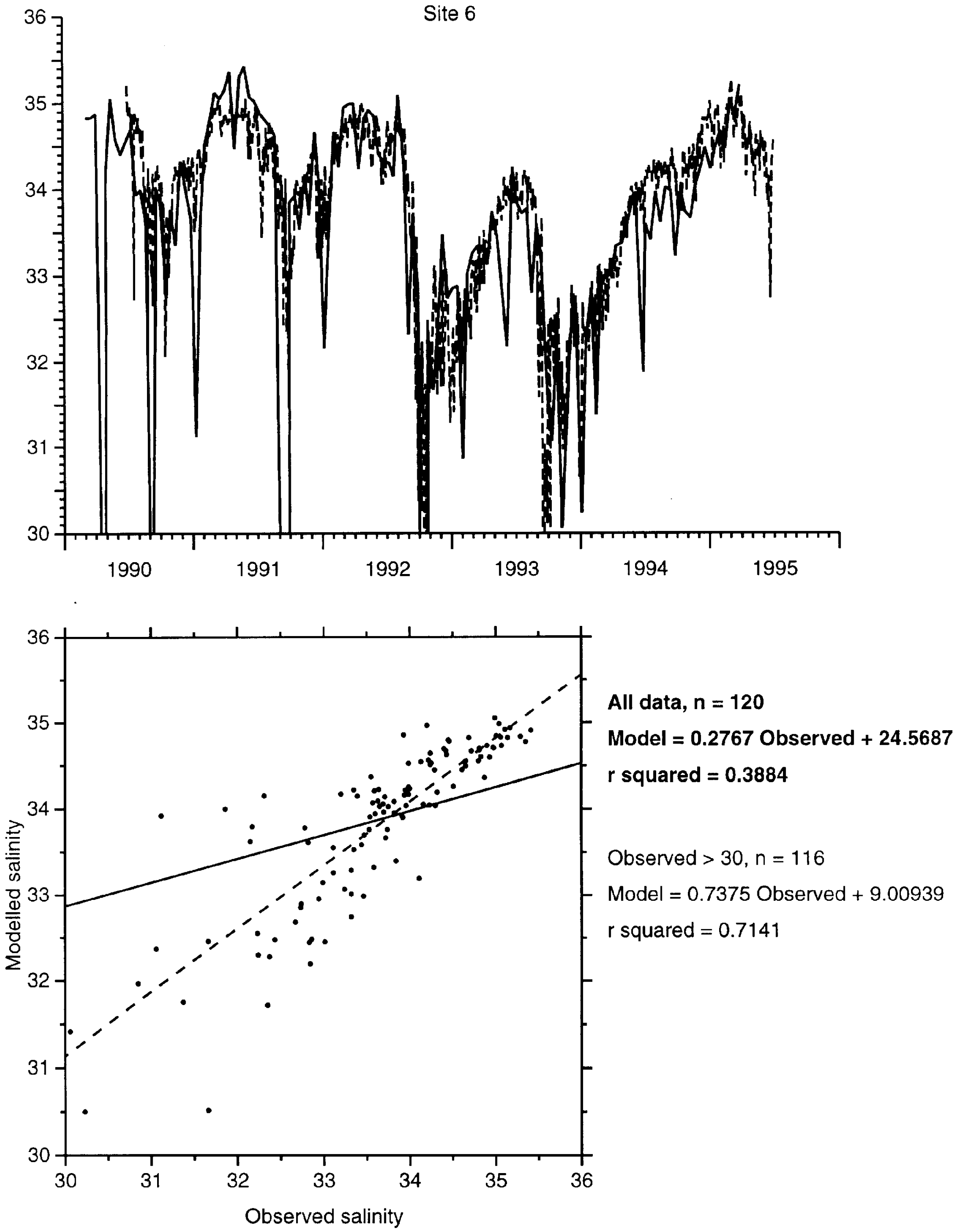

Figure 20: The upper plot shows time series of measured (solid line) and modelled (dashed line) salinities at Site 6 over the period 1990 to 1995. For this simulation, rainfall inputs were scaled by a factor of 1.6. The lower plot shows a scatter plot of these salinity data, together with linear regression values and lines of best fit for both all data (solid line and bold text) and for measured values greater than or equal to 30 (dashed line and normal text) .

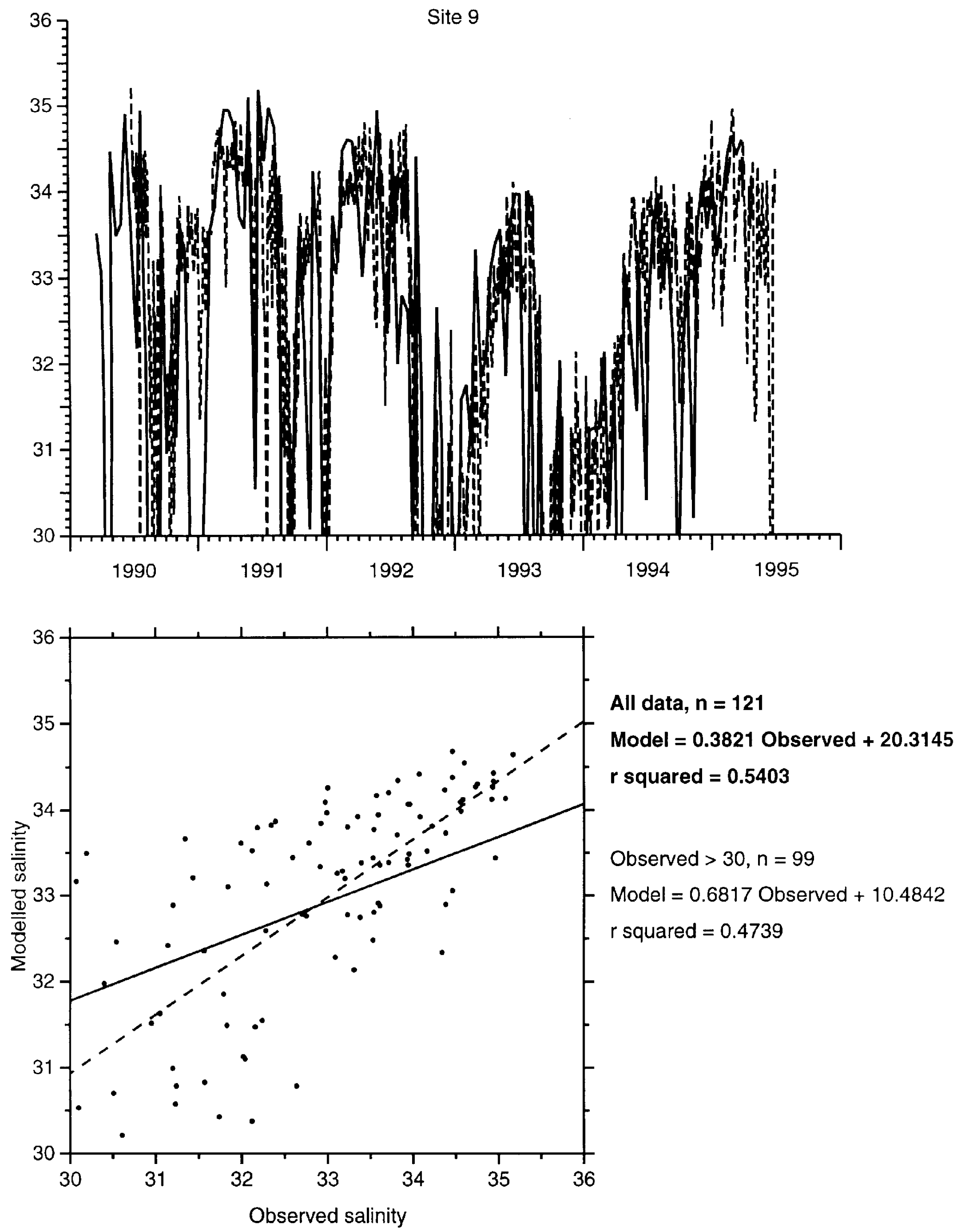

Figure 21: The upper plot shows time series of measured (solid line) and modelled (dashed line) salinities at Site 9 over the period 1990 to 1995. For this simulation, rainfall inputs were scaled by a factor of 1.6. The lower plot shows a scatter plot of these salinity data, together with linear regression values and lines of best fit for both all data (solid line and bold text) and for measured values greater than or equal to 30 (dashed line and normal text).

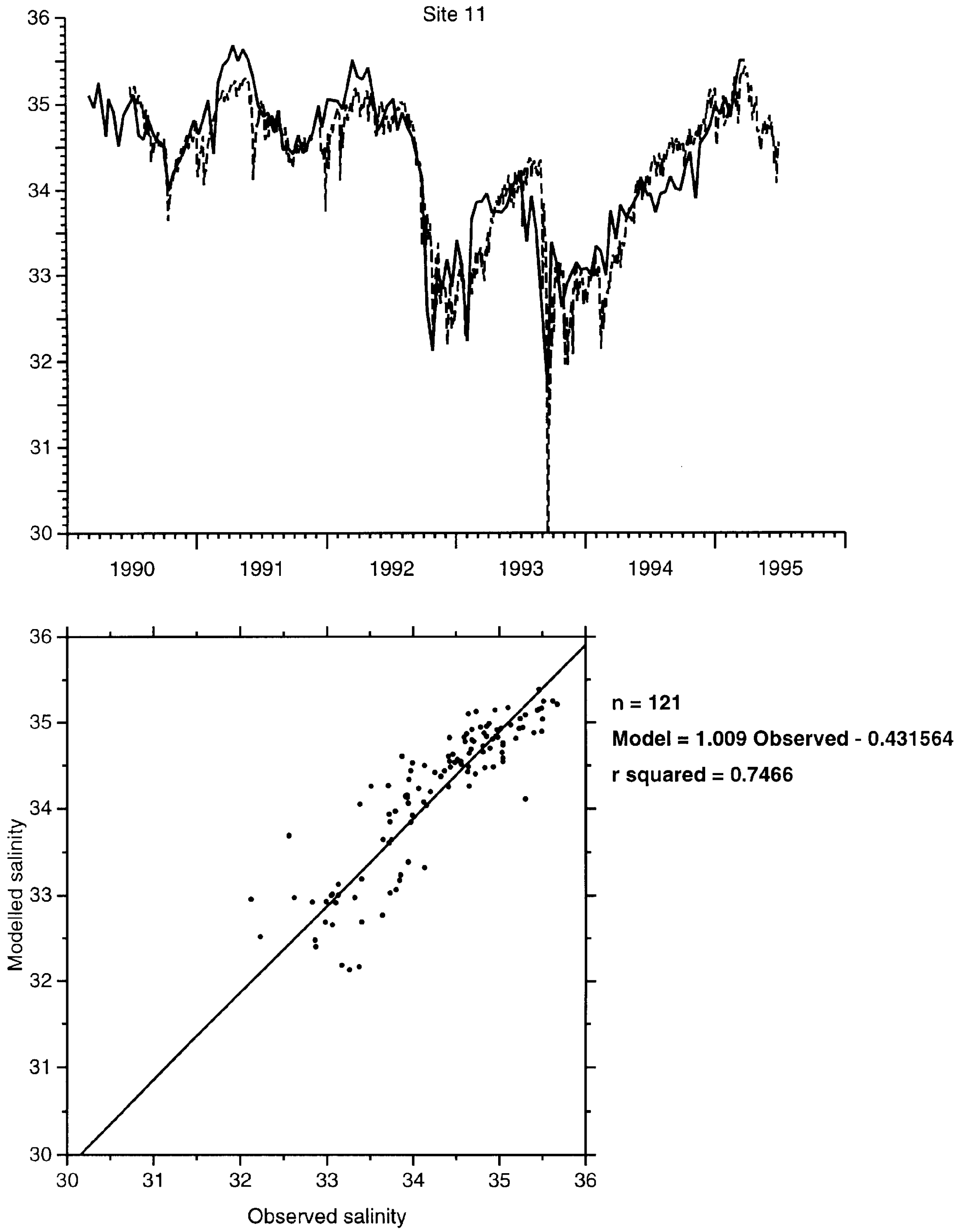

Figure 22: The upper plot shows time series of measured (solid line) and modelled (dashed line) salinities at Site 11 over the period 1990 to 1995. For this simulation, rainfall inputs were scaled by a factor of 1.6. The lower plot shows a scatter plot of these salinity data, together with linear regression values and line of best fit.

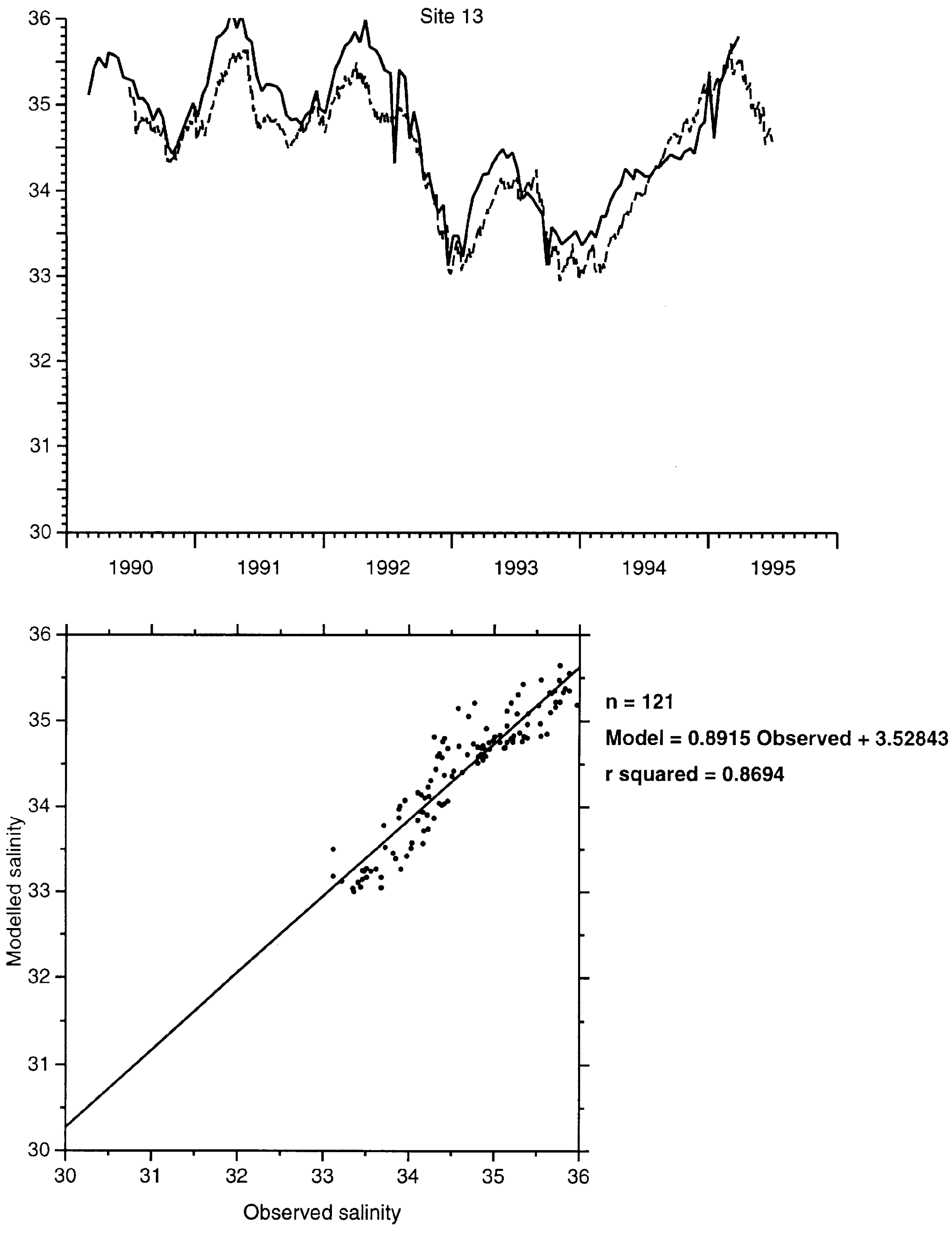

Figure 23: The upper plot shows time series of measured (solid line) and modelled (dashed line) salinities at Site 13 over the period 1990 to 1995. For this simulation, rainfall inputs were scaled by a factor of 1.6. The lower plot shows a scatter plot of these salinity data, together with linear regression values and line of best fit.

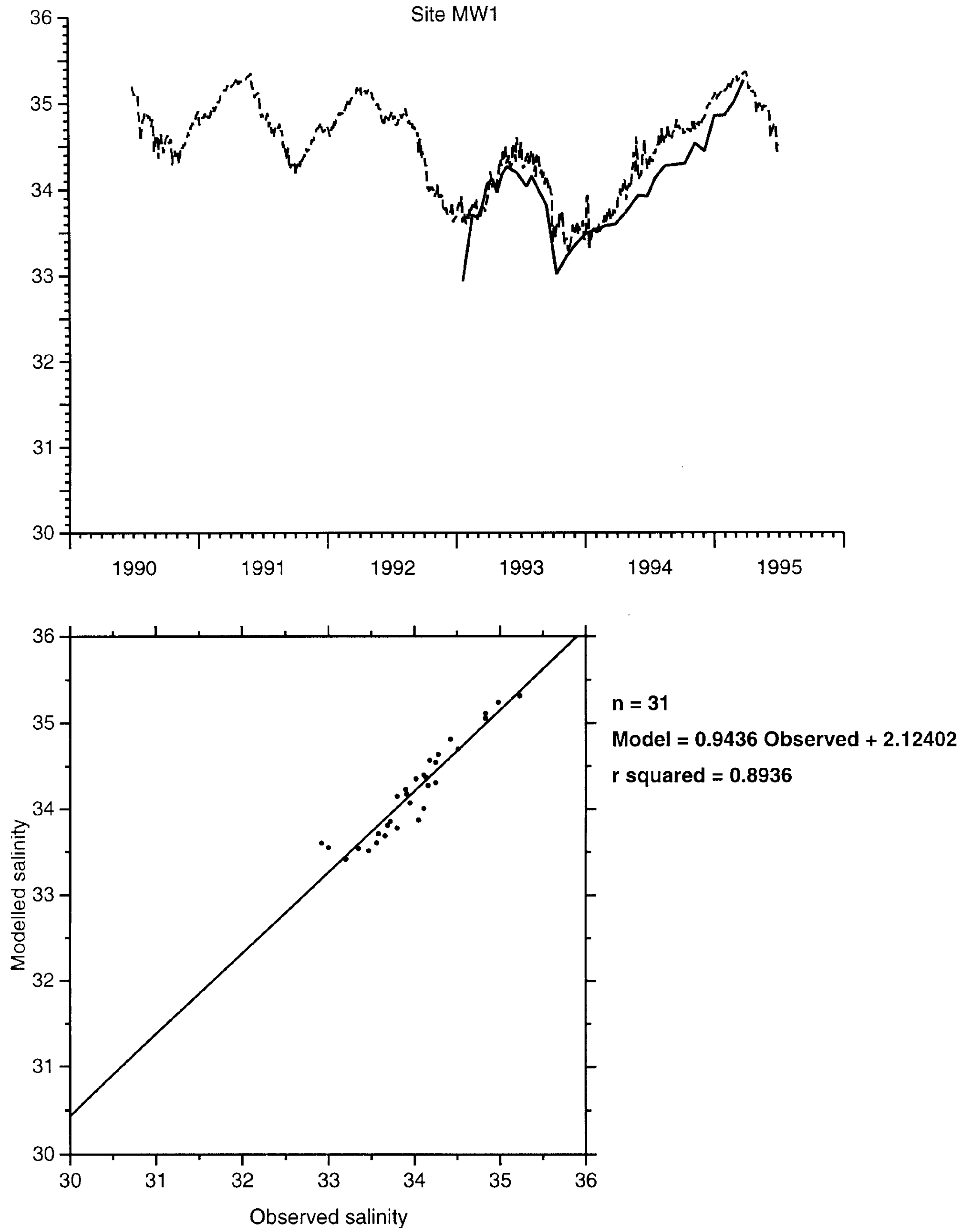

Figure 24: The upper plot shows time series of measured (solid line) and modelled (dashed line) salinities at Site MW1 over the period 1990 to 1995. For this simulation, rainfall inputs were scaled by a factor of 1.6. The lower plot shows a scatter plot of these salinity data, together with linear regression values and line of best fit.

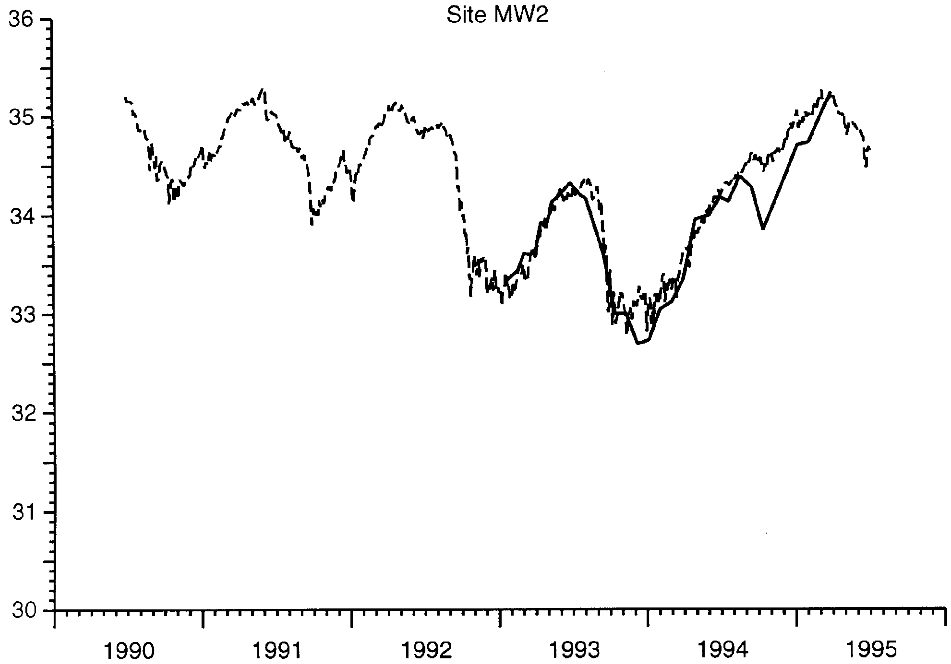

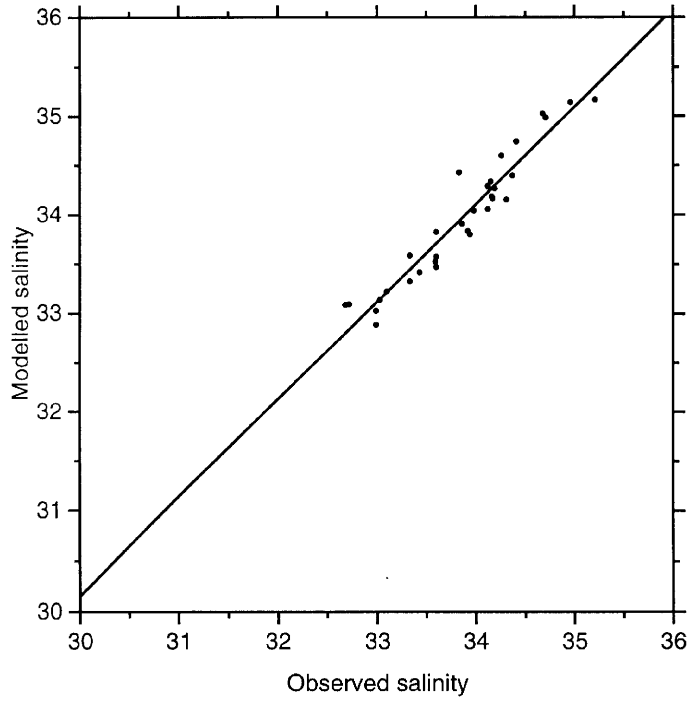

n = 32

Model = 0.9876 Observed + 0.526763

r squared = 0.9186

Figure 25: The upper plot shows time series of measured (solid line) and modelled (dashed line) salinities at Site MW2 over the period 1990 to 1995. For this simulation, rainfall inputs were scaled by a factor of 1.6. The lower plot shows a scatter plot of these salinity data, together with linear regression values and line of best fit.